Strål säkerhets myndigheten
Swedish Radiation Safety Authority

Author: Ali R. Massih

Research

2014:20

An evaluation of high-temperature creep of zirconium alloys: data versus models

Report number: 2014:20 ISSN: 2000-0456
Available at www.stralsakerhetsmyndigheten.se

SSM perspective

Background

The materials that constitute the nuclear fuel rods are under constant development to meet higher expectations on safety and efficiency. Cladding material shall be more resistant against effects of irradiation and failures. For example, zirconium alloys with niobium have become widely used due to their improved resistance to corrosion (these so called Zr1%Nb materials are for example M5, ZIRLO and E110). Alongside hardware improvements, analytical tools are developed to include capabilities to analyze new materials. For analysis of nuclear fuel behavior, it is necessary to have reliable tools, in this case, computational codes with models for relevant physical phenomena.

Criteria for reliable tools are that they shall be verified against experimental data. Furthermore, comparisons with codes from other institutes and developers, accompanied with a fundamental understanding of the differences will also indicate reliability of these codes.

Objectives

Material properties, for example creep, are temperature dependent; at lower temperatures the material is harder whereas at higher temperatures it is softer. The material resides in different crystal structures (phases) at low and high temperatures and in between there is a region of transition. The transition region (coexistence phase) is difficult to model and each fuel developer has its own model and correlation to describe the creep of the material.

The compilation of information in this report describes the common properties of similar materials from different suppliers which are a valuable step for comparing materials and models.

Results

In this report Dr Massih presents correlations for creep in different phases of zirconium alloys and also presents a general solution to the difficulty of accurately describing the material properties in phase transition for several zirconium alloys. Based upon superplasticity relations, models are adapted to fit with experimental data for materials in transition regions. The creep models are developed for both previous generations of zirconium alloys (Ziracaloy-2 and Zircaloy-4) and upgraded to fit for Zr1%Nb materials. The adaptations are successful since a good agreement between experimental data and model computation has been reached, based on a better understanding of the physical phenomena acting in the materials.

Need for further research

Ongoing research in, for example, Halden and at Studsvik is addressing fuel behavior. Currently, response of fuel rods to different operational stresses (integral tests) and tests of separate effects like creep and fission

gas release are being performed. This research will address behavior of new materials and issues arising from irradiation. Modeling and code development will to a large extent determine how the tests shall be designed.

Project information
Contact person SSM: Anna Alvestav
Reference: 2008/139

Strål
säkerhets
myndigheten
Swedish Radiation Safety Authority

Author: Ali R. Massih
Quantum Technologies AB, Uppsala, Sweden

2014:20

An evaluation of high-temperature creep of zirconium alloys: data versus models

Date: April 2014
Report number: 2014:20 ISSN: 2000-0456
Available at www.stralsakerhetsmyndigheten.se

This report concerns a study which has been conducted for the Swedish Radiation Safety Authority, SSM. The conclusions and viewpoints presented in the report are those of the author/authors and do not necessarily coincide with those of the SSM.

Contents

Abstract

The steady-state creep data of as-received Zircaloy-4 and Zr-1wt%Nb used as fuel cladding materials in light water reactors, reported in the literature, have been reappraised. The considered creep tests were conducted in the temperature range from 923 to 1873 K in inert environment covering all the solid-state zirconium alloy stable phase domains: α, $(\alpha + \beta)$ and β as a function of applied stress. The results of model calculations and measured data are compared, where the relative difference between the measured and calculated creep rate values are quantified for a series of tests. The models considered are those used or can be used in predictive computer codes for fuel rod behaviour under loss-of-coolant accident conditions in light water reactors.

Sammanfattning

Stationära krypdata för obestrålad Zircaloy-4 och Zr1%Nb, som används i kapslingsrör till kärnbränslestavar i lättvattenreaktorer, rapporterade i litteraturen, har prövats på nytt. De beaktade kryptesterna utfördes i temperaturintervallet från 923 till 1873 K i inert miljö täckande samtliga stabila fasområden hos zirkoniumlegeringar: α, $(\alpha + \beta)$ och β som funktion av pålagd spänning. Resultat från modellberäkningar och mätdata jämförs, varvid den relativa skillnaden mellan uppmätta och beräknade värden på kryphastighet kvantifieras för en serie av tester. Modeller som beaktas är sådana som används eller skulle kunna användas i datorprogram för uppskatting av bränslestavbeteende under förhållanden rådande vid en olycka orsakad av kylmedelsförlust i lättvattenreaktorer.

1 Introduction

In a postulated loss-of-coolant accident (LOCA) in light-water reactors (LWRs), zirconium alloy fuel cladding tubes are subjected to high temperatures (> 700 K) and internal over pressures. These conditions can cause excessive outward expansion (ballooning) of the cladding tube, primarily by creep mechanisms, thus reducing the subchannel area available for flow of the coolant water, i.e. causing coolant blockage in the refilling and flooding stages of LOCA [1–3].

Detailed knowledge of creep strain rate of cladding tube as a function of stress and temperature is fundamental for analysis of cladding deformation during a postulated LOCA. Hence, the constitutive relation for cladding creep rate is an essential ingredient of a computer model dealing with transient fuel rod behaviour during LOCA conditions [4]. High temperature creep behaviour of Zr-base alloys pertinent to LOCA conditions has been a subject of several past and recent studies reported in the literature [5–7]. The objective of this report is to review these open literature data and models quantitatively, and compare the results of model calculations with measured data regarding creep rate versus applied stress at various temperatures.

In this work, the creep rate behaviour of as-received (unirradiated) zirconium alloys used as fuel cladding materials is examined in the temperature range 923 to 1873 K. As is well known, at cladding temperatures above 975 K, the creep behaviour of irradiated and unirradiated fuel cladding is expected to be identical [8–10]. In a postulated LOCA, the strengthening effect of irradiation diminishes since the zirconium alloy will be annealed. Moreover, the creep rate measurements evaluated here were obtained in an inert atmosphere and hence provide a data base unaltered by strengthening mechanisms such as those due to oxygen. Hence our analysis offers a base-line for subsequent studies on creep of pre-oxidized cladding materials in steam environments, directly relevant to high temperature LOCA conditions. We evaluate the steady-state creep [1] behaviour of Zircaloy-4 material with nominal chemical composition: Zr-base, 1.5Sn-0.2Fe-0.1Cr-0.12O by wt% and Zr1%Nb alloy with nominal chemical composition: Zr-base, 1.0Nb-0.14O by wt%, in the temperature range of interest.

Zirconium alloys in solid state undergo a phase transformation from the low temperature hexagonal closed-packed (hcp) α-phase to body-centred cubic (bcc) β-phase [11]. Solid state phase equilibria of Zircaloy-4 have been investigated experimentally by Miquet et al. [12], who reported a prevalence of four phase domains, namely, $(\alpha + \chi)$ up to 1081 K, $(\alpha + \beta + \chi)$ from 1081 to 1118 K, $(\alpha + \beta)$ between 1118 and 1281 K, and β-phase above 1281 K. Here, χ refers to the intermetallic hexagonal Laves phase $Zr(Fe,Cr)_2$, see e.g. ref. [13]. For the sake of illustration, we have depicted an *isopethal* (constant composition) section of Zircaloy-4 with only the oxygen concentration as a variable in figure 1.

The phase equilibria of the Zr-Nb-O system have recently been evaluated in [14]. Kaddour et al. [7] report that the starting temperature of the $\alpha \rightarrow (\alpha + \beta)$ transition, determined by a resistivity technique, for Zircaloy-4 is about 1093 K and for Zr1%Nb alloy around 1043 K. Similarly, the start of the $(\alpha + \beta) \rightarrow \beta$ transition is about 1250 K for Zircaloy-4 and 1210 K for Zr1%Nb.

The high-temperature β phase is known to be "softer" than the low-temperature α phase in zirconium alloys, hence it is valuable to have knowledge of the stress dependence of the

[1] Steady-state creep is time-dependent plastic strain which occurs at a constant rate when the applied stress is kept constant.

creep in the former phase. It is worth mentioning that because of the low solubility of niobium in zirconium at low temperature, the Zr1%Nb alloy contains a few percent of β phase even at low temperature. This small amount of β phase dispersed as metastable particles, in a sea of α phase does not affect the deformation behaviour of Zr1%Nb according to ref. [7]. Thus, the low-temperature domain (α + a few percent of dispersed β phase) is still considered as the α domain in the Zr1%Nb alloy.
Garde et al. [15] have studied the uniaxial stress-strain behaviour of Zircaloy-2 and Zircaloy-4 specimens over the range of experimental conditions: 973-1673 K, strain rates $10^{-6} - 10^{-1}$ s^{-1} and oxygen concentrations 0.11-2.0 wt%, pertinent to LOCA conditions. They observed a superplastic behaviour, characterized by peaks in axial (elongation) strain of the specimen close to 1123 K. Elongation peaks are typical for a superplastic material in which most of the total strain results from the necking strain that follows uniform elongation in uniaxial tests.
The organization of this report is as follows. Section 2 presents the creep rate measurements in the α, $(\alpha + \beta)$ and β domains for Zircaloy-4 and Zr1%Nb cladding materials. The creep constitutive relations are described in section 3. In section 4, we evaluate the measured data with the aid of the models presented in section 3. Section 5 is devoted to discussion of the main results and section 6 concludes the report.

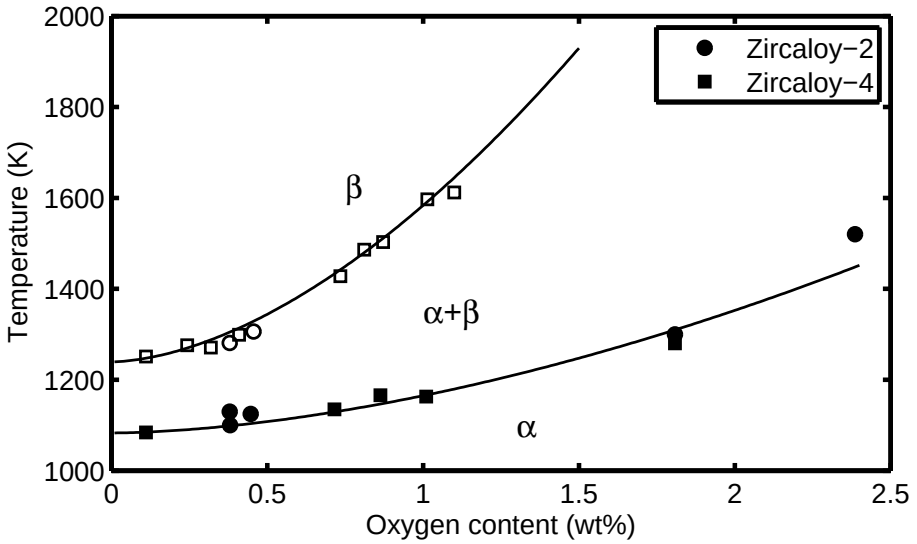

Figure 1: An isopethal section of Zircaloy phase diagram versus oxygen concentration [16]. The data were obtained from resistivity measurements.

2 Creep tests

In this section the results of creep tests performed on Zircaloys (primarily Zircaloy-4) and Zr-1%Nb cladding tube materials in the α phase, the coexisting ($\alpha + \beta$) phase and pure β phase are presented. For Zr-1%Nb the published data are very limited, but since zirconium alloys containing Nb are prevalent as fuel cladding materials presently, their assessment is relevant.

2.1 Zircaloy data

The creep behaviour of as-received Zircaloy-4 fuel cladding in the temperature range of 940 to 1873 K were comprehensively assessed in a 1978 report [8] and a subsequent publication [5] by workers at the Atomic Energy of Canada Research Company, Whiteshell Nuclear Research Establishment, Manitoba, Canada. The data presented in [8] include both published and unpublished creep data available up to 1978 in the high temperature α-Zr, the β-Zr and the coexisting ($\alpha+\beta$) phase obtained by uniaxial creep testing. In this context, we have also included the recent data obtained by researchers at Ecole des Mines de Paris and CEA Saclay, France [7] on Zircaloy-4 at 973 K and 1273 K. Finally, we present data reported by Donaldson and colleagues [6] of the Berkeley Nuclear Laboratories, UK, on the biaxial creep deformation of as-received Zircaloy-4 fuel cladding in the α, ($\alpha + \beta$) and β phase temperature ranges.

2.1.1 Rosinger et al. 1978-1979

The uniaxial creep tests reported in [5, 8] were conducted in an inert atmosphere in order to obtain a set of Zircaloy-4 data, which were unaffected by strengthening due, for example, to oxygen. They provide a base-line set of data for modelling creep behaviour which separate the effect of oxidation on creep. In fact, creep of Zircaloy-4 was studied independently at two laboratories, namely, by W.R. Clendening at Westinghouse Canada Ltd. and by Rosinger and Bera at the Atomic Energy of Canada Ltd. (AECL) which is reported in [5, 8]. The two investigations used the same material and utilized the same experimental approach.

The isothermal tests by Rosinger and coworkers were made in an argon atmosphere using axially-symmetric Zircaloy-4 fuel cladding with nominal mean diameter of 15.24 mm and wall thickness of 0.44 mm. The cladding was in as-received condition with 70% area reductions followed by 4 hour stress relief at about 795 K and then furnace cooling.

A schematic of the test apparatus employed by Rosinger et al. [8] is shown in figure 2. It consists of a cylinder chamber with a diameter of 200 mm and a height of 500 mm. The applied load (stress) levels in the α phase ranged from 11.30 to 42 MPa, in the ($\alpha + \beta$) phase, they were in the range 1.5 to 60 MPa, whereas in the β phase they were from 1.2 to 10.2 MPa.

The specimen was heated directly (Joule or ohmic heating) and the load cell and the test chamber were electrically insulated from the test sample. The test chamber was mounted on a so-called Material Test System (MTS) servo-hydraulic apparatus, which was used to apply the constant uniaxial load to the sample and to measure the strain of the sample at constant load and temperature. The strain of the sample was determined by measuring the displacement of the MTS ram by means of a linear variable differential transformer

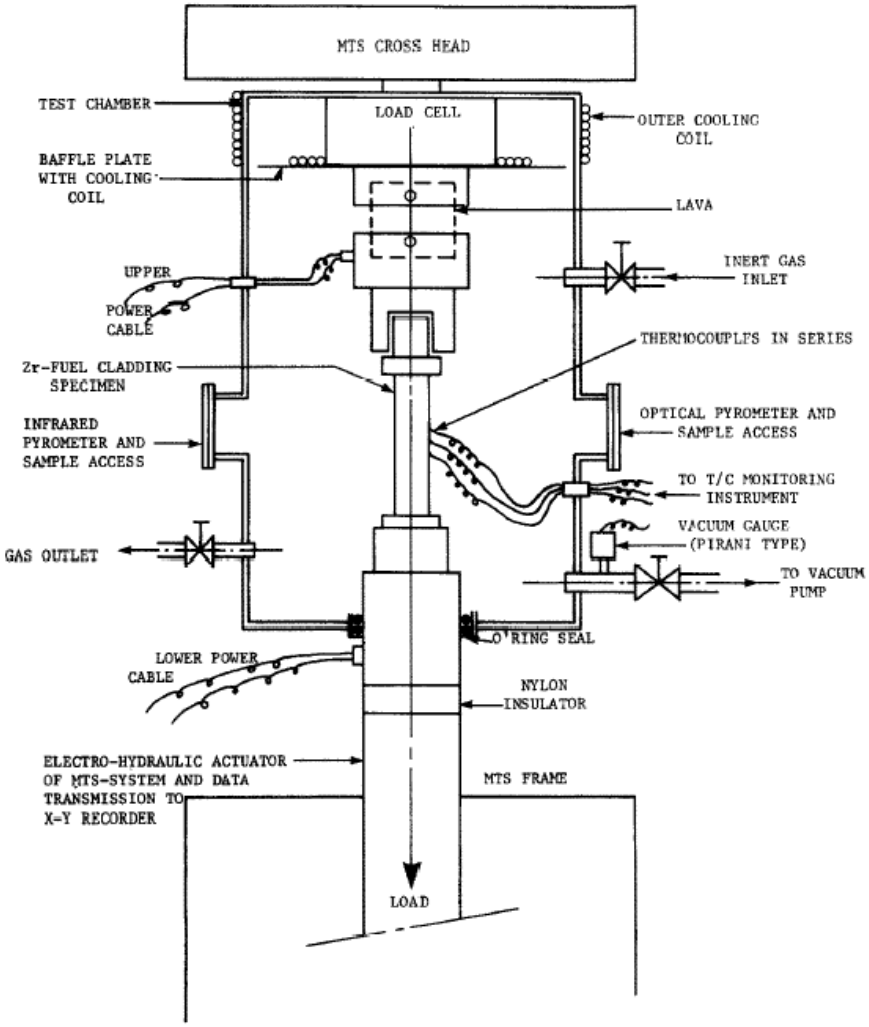

Figure 2: A schematic of the creep testing apparatus [8].

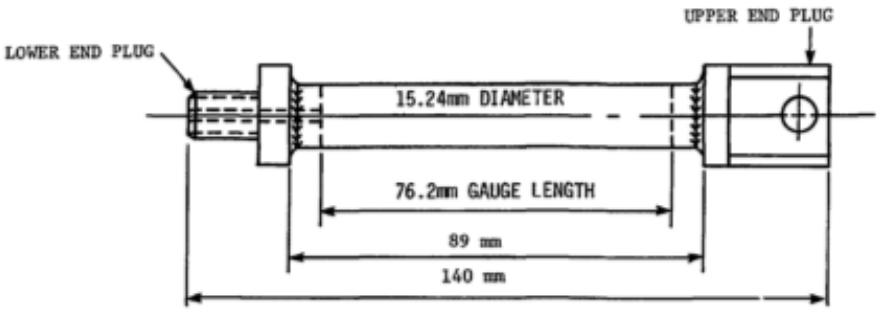

Figure 3: Creep test specimen [8].

Table 1: Isothermal creep tests of Zircaloy-4 matrix in the α phase. All the test results (figure 4b) can be found in [8], except the data of Kaddour, which are presented in [7].

Temperature K	Stress range MPa	Worker ...
940	47.5-58.6	Clendening
973	20.7-27.6	Chung et al.
973	8.3-47.4	Kaddour et al.
990	33.9-56.8	Clendening
1033	23.6-26.9	Busby & Marsh
1040	22.0-46.4	Clendening
1073	20.7-27.6	Chung et al.
1075	8.96-24.78	Busby & White
1075	19.6 -24.8	Busby & Marsh

(LVDT). The ram displacement was recorded as a function of time. A section of Zircaloy-4 cladding, 89 mm long, was welded with two end fittings in argon atmosphere (figure 3). Thermocouples were tack-welded at and near the centre of the outer surface of the sample's gauge length.

Upon installing the test apparatus, Rosinger and co. evacuated the vessel to a vacuum of 0.67 Pa and then backfilled it with high-purity argon flowing through a titanium getter system to further remove contamination. This procedure was repeated several times before a steady flow of inert gas was introduced. An AC electric power supply was utilized for heating the samples at the rates 50 to 100 K/s to their test temperatures. The test temperature was measured by the thermocouples, which was attained in about 10-20 s with a further 10-20 s delay before loading. After stabilization of temperature, the load was applied to a prescribed level in one second for most of the tests. The creep test was terminated after either 10 minutes had passed or a strain of 0.15 had been reached. At the end of the creep test at target temperature, the loading and heating were stopped and the sample was allowed to cool to ambient temperature. The total strain of the samples was then measured and compared with the strain-time data.

Rosinger et al. [8] test facility allowed a continuous recording of strain versus time for each sample tested. A polynomial fitting of strain versus time data was made for each sample from which the instantaneous strain rate was obtained by numerical differentiation.

The results of the creep rate versus stress and temperature in the α phase ($940 \leq T \leq 1075$ K) are displayed in log-log diagrams, figures 4a-b. The results for ($\alpha + \beta$) phase ($1090 \leq T \leq 1190$ K) are presented in figure 5. The data at 1098 K belong to Zr-0.7 wt%Sn specimens. The corresponding data in the β phase ($1255 \leq T \leq 1873$ K) are displayed in figure 6. The sources of the data in figures 4b, 5 and 6b are presented in tables 1, 2 and 3, respectively. Figures 4b and 6b also include the results of the recent experiment of Kaddour et al. [7] on Zircaloy-4 at 973 K and 1273 K, respectively.

Kaddour et al. [7] creep tests at *Ecole des Mines de Paris* included tests on stress-relieved Zircaloy-4 (Zr-1.5Sn-0.2Fe-0.1Cr-0.1O by wt%) with equiaxed grains of a mean size of 8 μm and a melting point of 2120 K. The specimens tested were from a fuel cladding tube with an outer diameter of 9.50 mm and a wall thickness of 0.57 mm. The procedure of the creep test is described in section 2.2. During the creep tests, Kaddour and company investigated the effects of loading history by increasing then decreasing load levels by

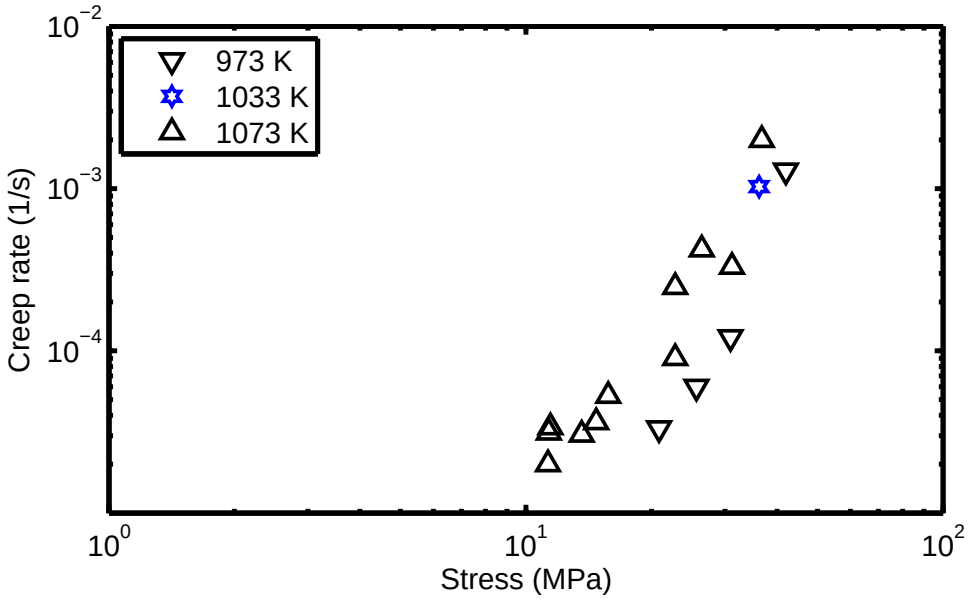

(a)

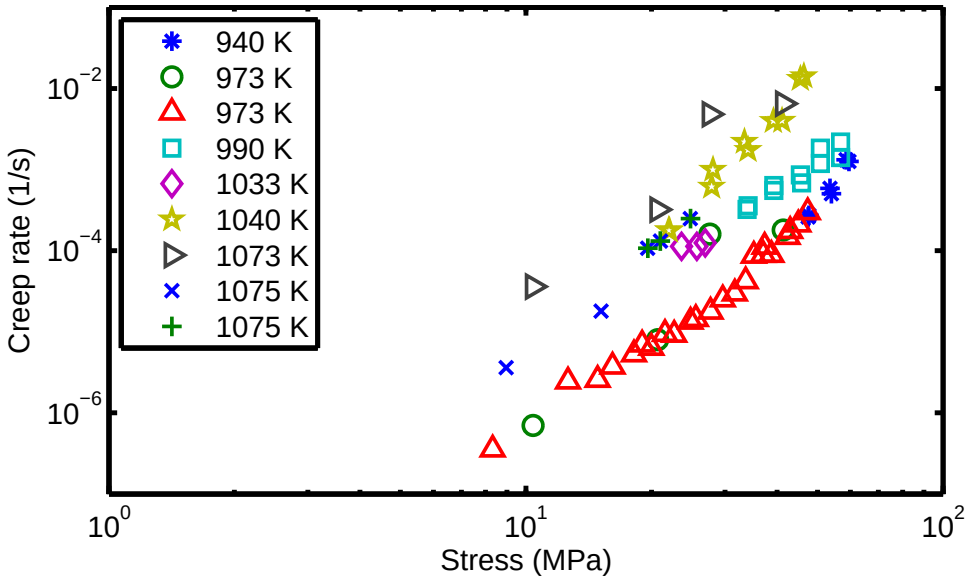

(b)

Figure 4: Measured axial creep strain rate versus nominal axial stress for Zircaloy-4 cladding samples in the α phase, (a) AECL own data [8], (b) Other workers data presented in [8], see table 1. The upward (red) triangle data at 973 K are those of Kaddour et al. [7].

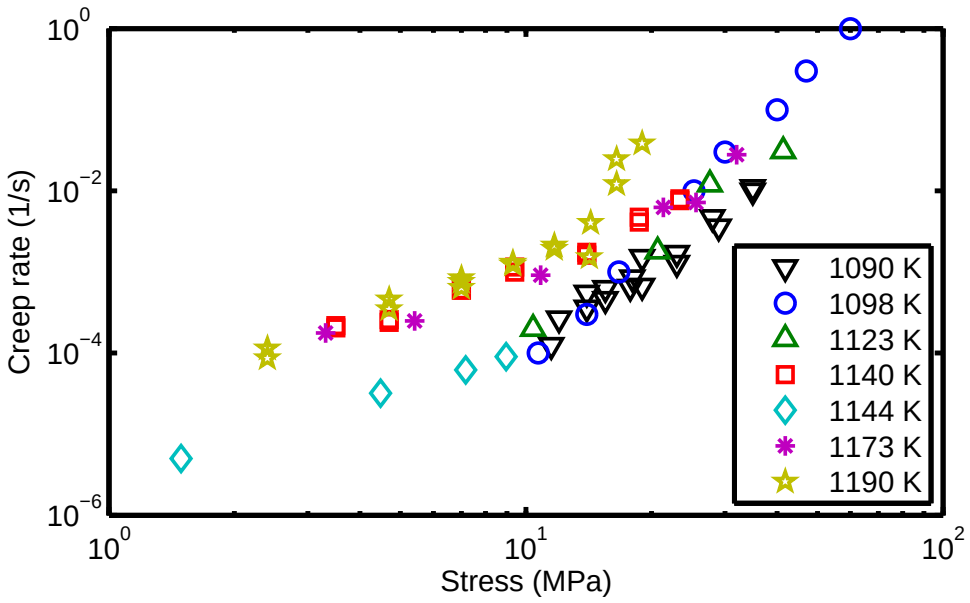

Figure 5: Measured axial creep strain rate versus nominal axial stress for Zircaloy-4 and Zr-0.7 wt%Sn (1098 K) cladding samples in the $(\alpha + \beta)$ phase, after [5, 8], see table 2.

Table 2: Isothermal creep tests of Zircaloy-4 matrix in the $(\alpha + \beta)$ phase. All the test results (figure 5) can be found in [8], except that of Rosinger, which are presented in [5].

Temperature K	Stress range MPa	Worker ...
1090	11-35	Clendening
1098	10.7-60	Luton & Jonas (Zr-0.7 wt%Sn)
1123	20-41	Chung et al.
1140	3.5-23.4	Clendening
1144	1.49-9.0	Busby & White
1173	3.3-32	Rosinger
1190	2.4-19	Clendening

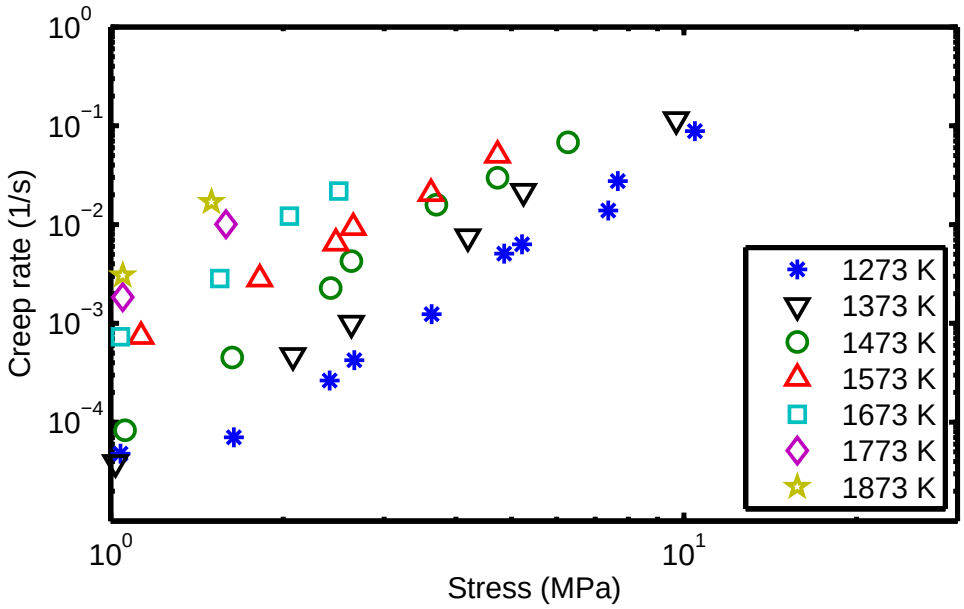

(a)

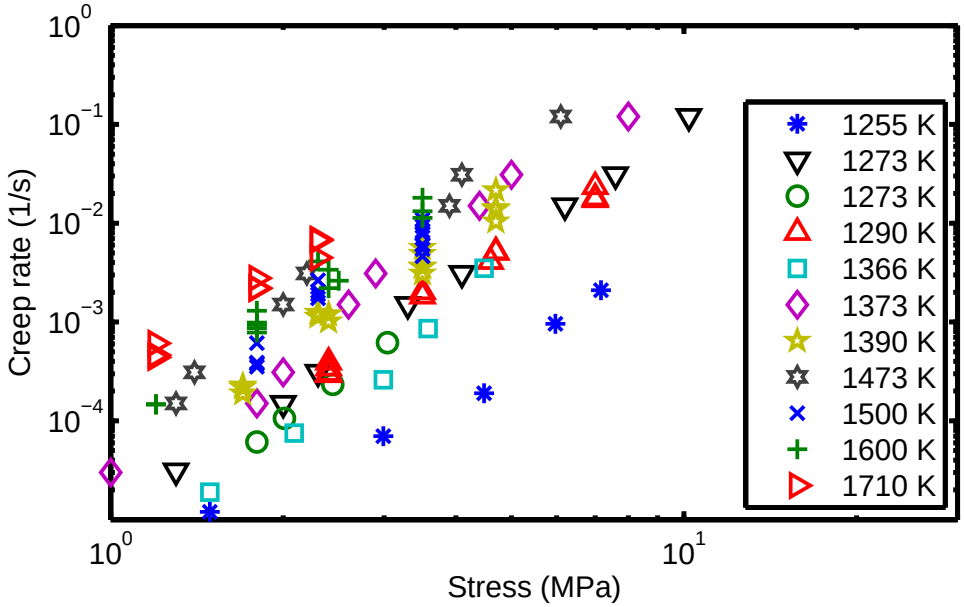

(b)

Figure 6: Measured axial creep strain rate versus nominal axial stress for Zircaloy-4 cladding samples in the β phase, (a) AECL own data [8], (b) Other workers data presented in [8], see table 3. The open circle data at 1273 K are those of Kaddour et al. [7].

Table 3: Isothermal creep tests of Zircaloy-4 matrix in the β phase. All the test results (figure 6) can be found in [8], except that of Kaddour et al. [7].

Temperature K	Stress range MPa	Worker ...
1255	1.5-7.2	Busby & White
1273	1.3-10.2	Rizkalla et al.
1273	1.8-3	Kaddour et al.
1290	2.4-7	Clendening
1366	1.5-4.5	Busby & White
1373	1-8	Rizkalla et al.
1390	1.7-4.7	Clendening
1473	1.3-6.1	Rizkalla et al.
1500	1.8-3.5	Clendening
1600	1.2-3.5	Clendening
1710	1.2-2.3	Clendening

small steps. They note that this was necessary, since the changes in microstructure, e.g. re-crystallization of α phase in stress relieved Zircaloy-4 or β-Zr grain growth, could have affected the creep behaviour of the alloy.

2.1.2 Donaldson et al. 1984-1985

Donaldson and coworkers [6, 17, 18] have examined the creep behaviour of Westinghouse Zircaloy-4 fuel cladding tubes of the 17×17 PWR design at temperatures between 973 and 1473 K using constant pressure biaxial creep tests. They present data on creep rates, cladding rupture strain and times to rupture as a function of stress and temperature. Here, we only consider their creep rate data. Sample cladding tubes with nominal dimensions of 9.5 mm outside diameter and 0.56 mm wall thickness were studied. Test samples, 760 mm long, were cut from as-fabricated tubing that was in stress relieved condition. A Pt-Pt/13 percent Rh thermocouple was spot welded to the inner surface of each tube sample at the mid-length plane, where diametral changes were measured during creep deformation. Donaldson et al. tested all the tube test samples under isothermal conditions at constant internal pressure using purified argon gas. Tests were continued until the rupture of the specimen. They evacuated the tube containment vessel to 5×10^{-3} Pa pressure.
In the two-phase coexistence domain, samples were heated electrically using a transformer to the test temperature within the $(\alpha + \beta)$ domain at a rate of 10 K/s and then kept at that temperature for 10 minutes (annealing time) before pressurizing the tubes and performing the creep testing. Additional annealing times at temperatures were used to examine the influence of this parameter on creep rate.
Their estimated axial temperature variations were ± 2 K over the central 350 mm of the test sample while the internal gas pressure was controlled to $\pm 7 \times 10^{-3}$ MPa for pressures in the range 0.1 to 8 MPa. They measured the increase in tube diameter during the test at a single position mid-way along the tube using a laser gauge. They report that the tube "distension" was uniform up to large strains before local ballooning and rupture occurred at a random position along the tube. The same test procedure was also utilized in β phase temperature range (1323 to 1473 K) on the cladding tube samples [6].

Donaldson et al. [6] calculated the true instantaneous radial strain $\varepsilon_{\rm ins}$ during deformation by means of the relation

$$\varepsilon_{\rm ins} = \ln\Big[\frac{r_{\rm i} + [r_{\rm i}^2 - (2r_0 - w_0)w_0]^{1/2}}{2r_0 - w_0}\Big], \tag{1}$$

where $r_{\rm i}$ and r_0 are the instantaneous and initial tube outer radius, respectively, as measured by the laser gauge, and w_0 is the initial cladding wall thickness. Typical strain versus time curves obtained by Donaldson and coworkers in the α, $(\alpha + \beta)$, and β phase are shown in figure 7.

We should note that according to the early works of Woodford [19, 20] a plot of the logarithm of the instantaneous creep rate versus strain should be linear in the region where steady-state creep prevails. In addition, extrapolating from the linear region onto $\log \dot{\varepsilon}_{\rm ins}$ axis gives the initial steady-state (secondary) creep rate, $\dot{\varepsilon_0}$. Donaldson and co. analyzed the creep curves obtained in the α and β phases using the Woodford method to determine $\dot{\varepsilon}_0$. An example of this kind of analysis is displayed in figures 7a and 7c for the α and β phases, respectively. In the coexistent $(\alpha + \beta)$ domain the log strain rate versus strain plot exhibits a point of inflection at which the instantaneous strain rate reaches a minimum value $\dot{\varepsilon}_m$ as can be seen from figure 7b.

Creep deformation in the mono phases α and β exhibited a power law stress dependence [6]. The steady-state creep rate $\dot{\varepsilon_0}$ data reported by Donaldson and coworkers in the α phase and β phase refer to $\dot{\varepsilon_0} \propto \sigma_0^n$, where σ_0 is the initial stress and n is the stress exponent. In the coexistence $(\alpha + \beta)$ domain, however, values of the minimum creep rate $\dot{\varepsilon}_m$ versus σ_0 were presented as the variation of the steady-state creep rate. Figure 8 depicts the hoop creep strain rate versus hoop stress data in the α domain, $973 \leq T \leq 1073$ K [18], figure 9 displays the data in the $(\alpha + \beta)$ domain, $1098 \leq T \leq 1223$ K [17] and figure 10 the corresponding data in the β domain, $1323 \leq T \leq 1473$ K [6].

2.1.3 Tensile tests by Garde et al. 1977-1978

Garde and coworkers [15] selected both Zircaloy-2 and Zircaloy-4 sheet materials for their tensile tests. The specimens were cold-rolled and annealed with thicknesses 0.686 and 0.635 mm, and recrystallized grain size of 15 and 11 μm, respectively. They also included hot-rolled and annealed Zircaloy-4 plate 6.35 mm in thickness. They subjected the plate to a cold-rolling and vacuum annealing sequence that resulted in an average recrystallized grain size of 5 μm in the 0.63 mm thick sheet. They machined tensile specimens with nominal gauge lengths of 25.4 and 12.7 mm (gauge widths of 6.53 and 3.18 mm) from the sheets according to the ASTM standard E8-69. They conducted the tests on a Model 1125 Instron testing machine [21]. The crosshead of the testing machine was equipped with a high temperature vacuum furnace with tungsten heating. The furnace was capable of maintaining a vacuum of 1.3×10^{-3} Pa at 1673 K. They held each sample for at least ≈ 10 minutes at temperature before deformation.

Garde and company measured the specimen temperature by a Pt-10% Rh thermocouple at a maximum distance of about 1 mm from the centre of the original gauge length. They converted the load-elongation data to engineering stress-strain values using the original cross-sectional area, original gauge length ℓ_0 and the instantaneous length ℓ; with strain defined as $(\ell - \ell_0)/\ell_0$. Subsequently, they obtained the true stress-strain data by a computer program that used the constant volume approximation. Tensile tests at variable speeds were

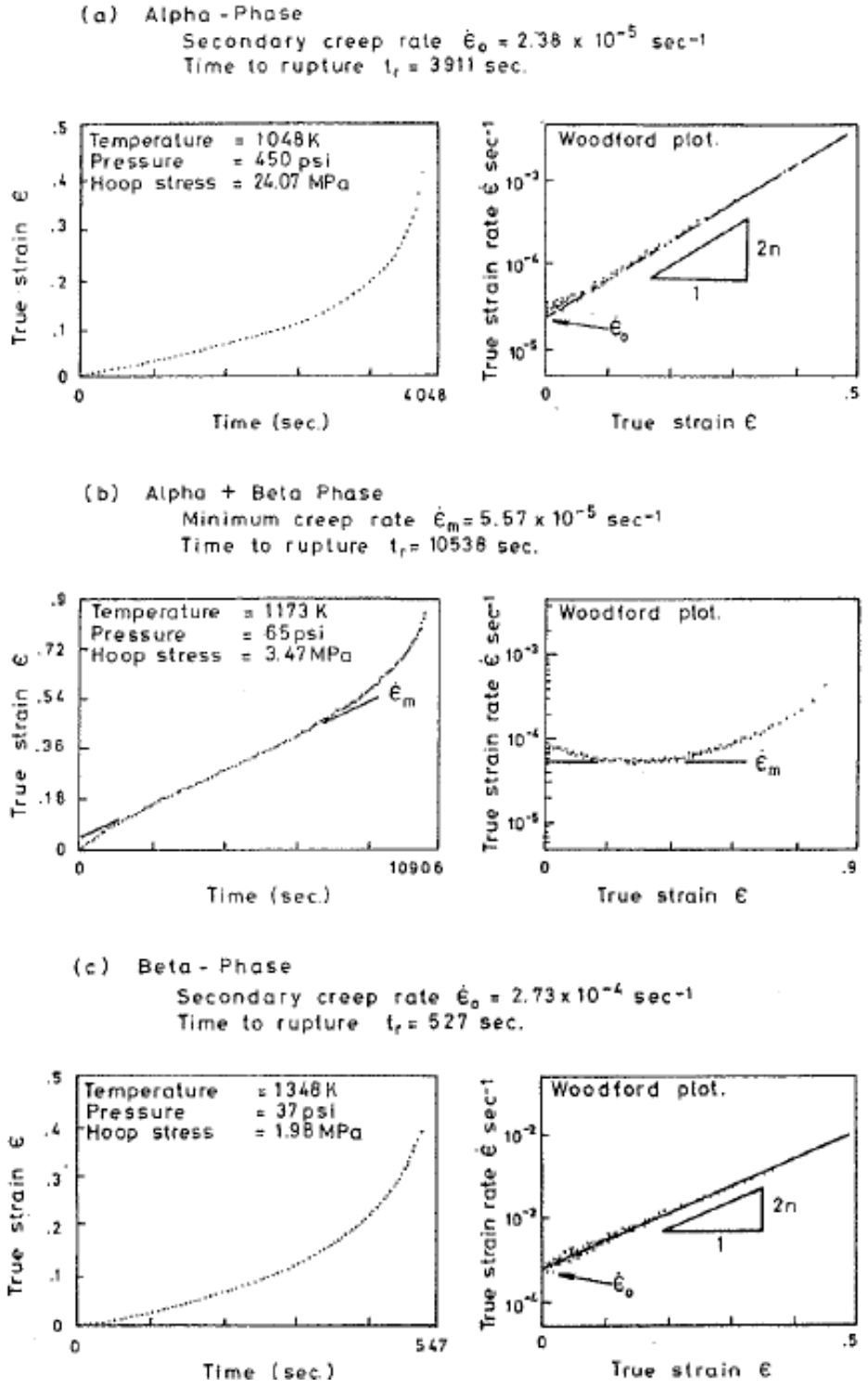

Figure 7: Strain versus time and log strain rate versus strain plots for Zircaloy-4 tube samples obtained by Donaldson et al. [6].

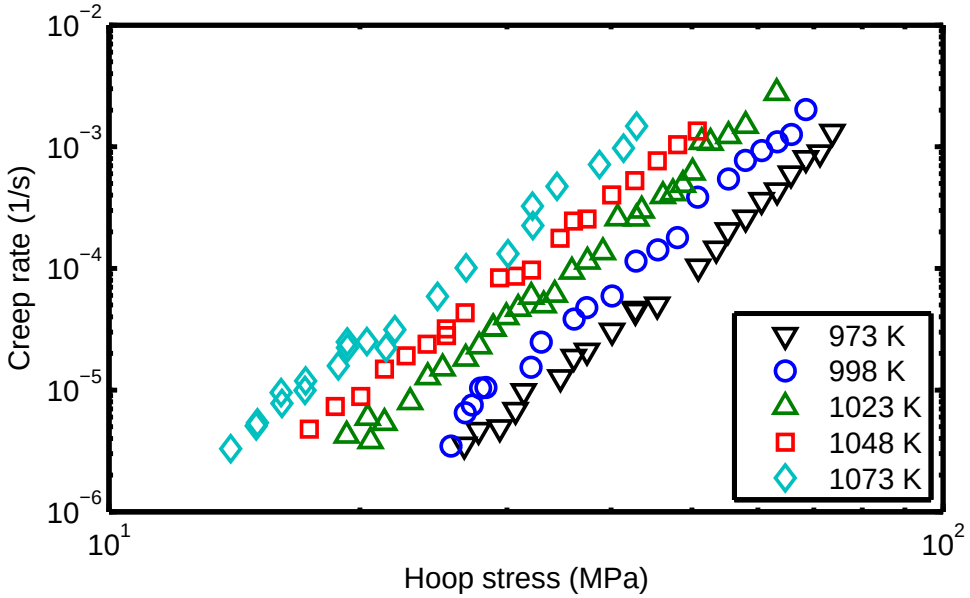

Figure 8: Measured creep hoop strain rate versus hoop stress for Zircaloy-4 cladding tube in the α phase, after [18].

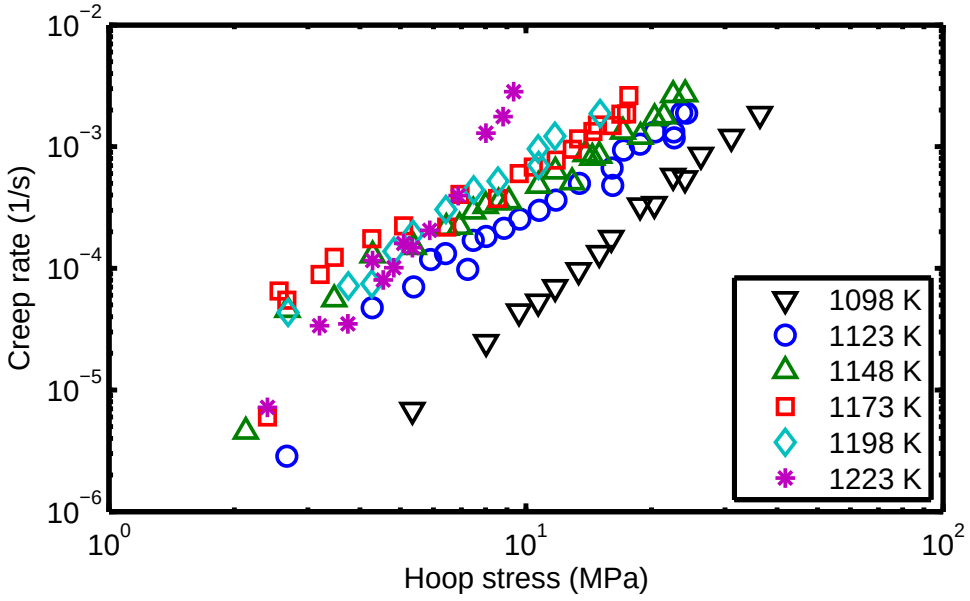

Figure 9: Measured creep hoop strain rate versus hoop stress for Zircaloy-4 cladding tube in the $(\alpha + \beta)$ phase, after [17].

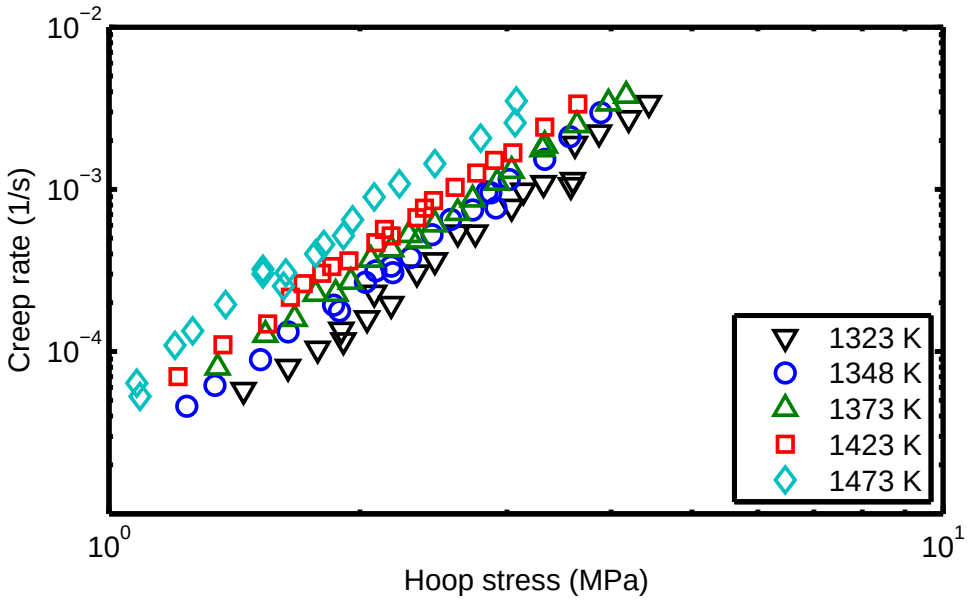

Figure 10: Measured creep hoop strain rate versus hoop stress for Zircaloy-4 cladding tube in the β phase, after [6].

conducted to determine the strain-rate sensitivity parameters. Garde et al. manifest their data in terms of the true stress-true strain relationship $\sigma = k\dot{\varepsilon}^m$, where k is a constant and m is the strain rate exponent. They refer to this true stress as the flow stress.[2]
Garde et al. [15] report that the Zircaloy-4 material exhibited superplastic total elongation peaks in the temperature range of 1073-1173 K and 1273-1323 K. For the two grain sizes (11 and 5 μm), the low temperature elongation peaks are separated by a minimum near 1223 K. Figure 11 shows a temperature dependence of the total strain at a strain rate of $\dot{\varepsilon} = 3.3 \times 10^{-4}$ s^{-1}. Here the total strain is defined as $(\ell_f - \ell_0)/\ell_0$ where ℓ_f is the specimen gauge length at fracture. Garde et al.'s experimentally determined strain rate versus the 0.2% yield stress for the two grain sizes at temperatures 1123 and 1173 K are presented in figure 12.

2.2 Zr1%Nb data

There is a scarcity of data on high temperature ($T > 640$ K) creep for Zr1%Nb and related zirconium alloys used for fuel cladding materials in the literature. One experimental work is the investigation by Kaddour et al. [7] at *Ecole des Mines de Paris*. Kaddour et al. [7] creep tests were done on re-crystallized Zr1%Nb with equiaxed grains of a mean size of 5 μm. The alloy chemical composition was typically (Zr-1.0Nb-0.14O by wt%) with a melting point of 2138 K. The specimens tested were from a fuel cladding tube with an outer diameter of 9.50 mm and a wall thickness of 0.57 mm, typical of 17×17 PWR fuel assembly cladding tube.

[2]The strain-rate-sensitivity parameter, m, is defined by $(\sigma_2/\sigma_1) = (\dot{\varepsilon}_2/\dot{\varepsilon}_1)^m$ where σ_1 and σ_2 are the flow stresses at strain rates $\dot{\varepsilon}_1$ and $\dot{\varepsilon}_2$, respectively. The strain-rate sensitivity m was determined from constant-temperature differential-crosshead velocity tests where a load change associated with a crosshead velocity change was measured at constant strain [21].

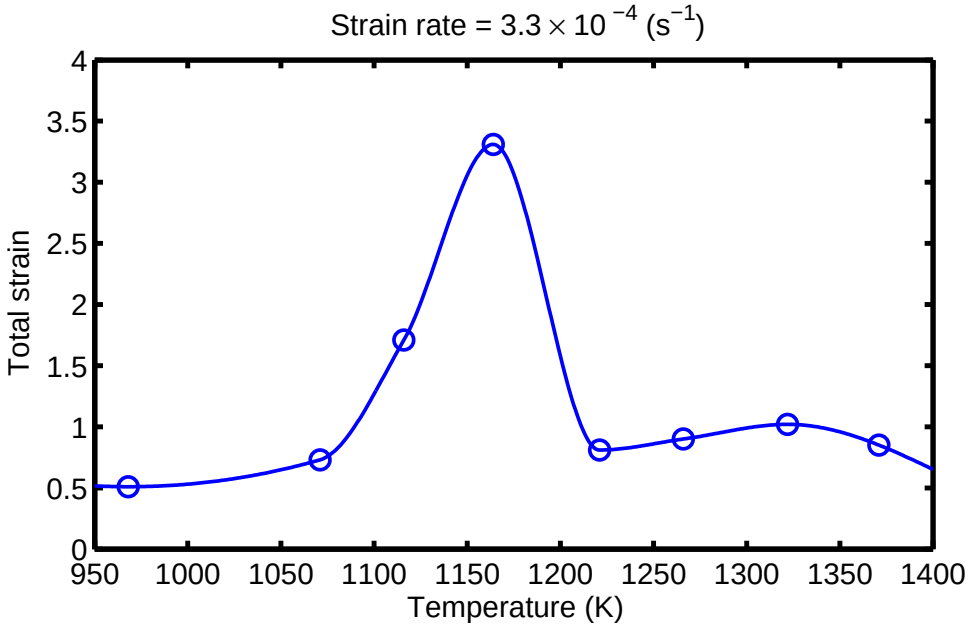

Figure 11: Measured total strain at different temperatures for 5 μm grain-size Zircaloy-4 specimen at strain rate of $\dot{\epsilon} = 3.3 \times 10^{-4}$ s^{-1}, after [15].

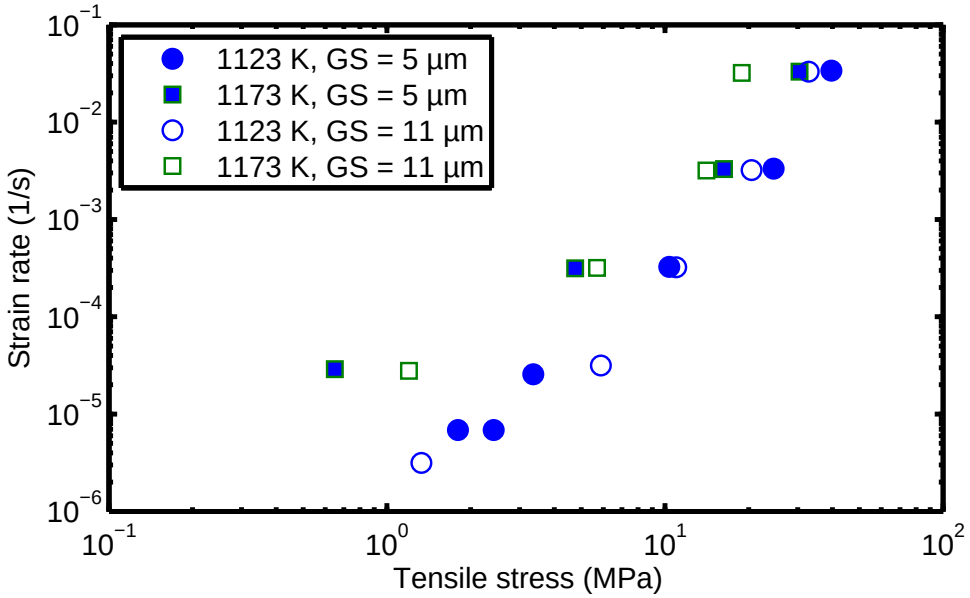

Figure 12: Measured strain rate versus the 0.2% yield stress at two temperatures and two grain sizes (GS) for the Zircaloy-4 specimens, after [15].

The creep tests (which also included Zircaloy-4 specimens) were conducted using an electrical-mechanical machine under load control, in which the tubes were tensile loaded along the axial direction [7]. Heating was done using a 6 kW radiation furnace inside a high vacuum chamber under $10^{-3} - 10^{-4}$ Pa. The temperature was monitored using Pt/Pt-10%Rh thermocouples spot-welded on the centre of the specimen. The axial elongation was continuously measured during the test using contact free laser extensometer. The 25-30 mm gauge length was delimited by utilizing two alumina rings attached onto the tube. The load was monitored using a 2 kN water cooled load cell positioned inside the vacuum chamber. The method for determining the strain rate from strain versus time is not described, however, it is noted that the steady state true strain rate, which was always (almost) attained immediately, was the same in loading and unloading conditions. Kaddour et al. [7] creep experiments also included electrical resistivity measurements to continuously monitor the phase transformation. The results of their measurements of strain rate versus temperature at different tensile stresses are shown in figure 13.

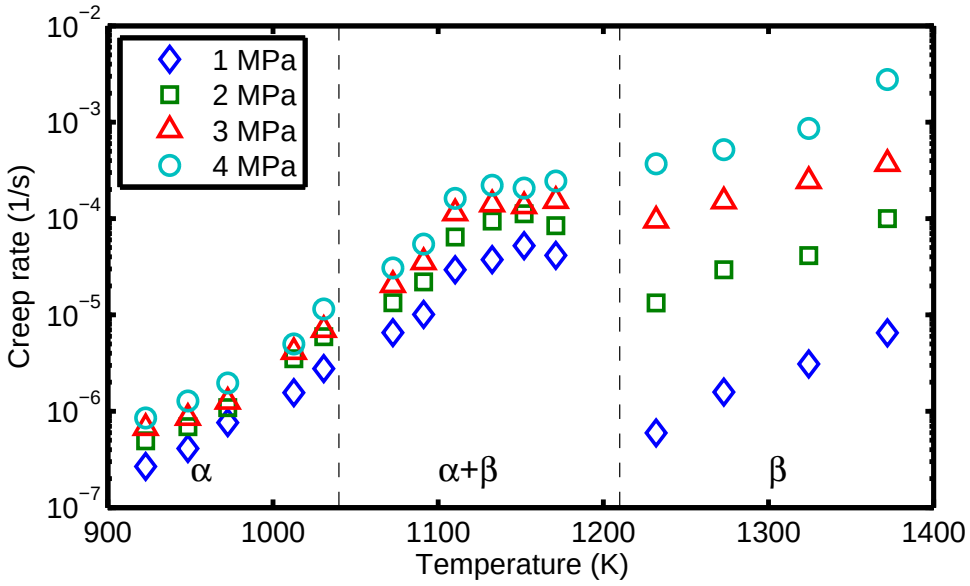

Figure 13: Measured axial true strain rate versus temperature covering $\alpha \rightarrow \beta$ domains of Zr1%Nb alloy at different axial tensile stresses, after [7].

3 Constitutive relations and mechanisms

The high temperature creep behaviour of Zr alloys are multifaceted. In the α phase domain ($T < 1040$ K for Zr-1%Nb and $T < 1090$ K Zircaloy-4), the experimental data [7] exhibit two creep regimes. At low stresses ($\sigma < 15$ MPa) the stress exponent parameter ($n \approx 1$) indicates that the deformation mechanism is diffusion creep, whereas at higher stresses ($\sigma > 15$ MPa), it is dislocation climb induced creep that controls creep deformation, i.e., n varies between 4 to 5. In the β phase domain, only dislocation climb induced creep ($n \approx 4$) has been observed.

In the two-phase coexistence $(\alpha + \beta)$ domain, however, the creep behaviour is more complex and as such no simple creep law has been established. Kaddour et al. [7] have observed that for very low applied stresses (1-2 MPa), strain rates in the $(\alpha + \beta)$ domain are substantially higher than those measured in the single-phase domains including the high-temperature region of the β-phase. The estimated stress exponent $n \approx 1$ given in [7] suggests that in the $(\alpha + \beta)$ domain the deformation mechanism could be controlled by inter-phase interface sliding, which is a signature for superplasticity [5, 15, 22–25].[3]

Superplasticity is intimately related to creep. As has been pointed out by Mukherjee [27], the three main requirements for superplastic behaviour are (i) fine (less than roughly 10 μm) and equiaxed grain structure that is fairly stable during deformation, (ii) a temperature which is higher than about half of the melting point of the solid, and (iii) a strain rate that is normally not too high (less than 0.001 s^{-1}) or not too low (more than 10^{-6} s^{-1}). These requirements are satisfied by nuclear grade Zircaloy materials in the $(\alpha + \beta)$ domain. For example, Kaddour et al.'s [7] Zircaloy-4 samples had equiaxed grains with a mean size of 5 μm.

In this section we describe the models that are used to evaluate the experimental data presented in the foregoing section. Many of the quantitative models used to describe the creep deformation of zirconium alloys are empirical/phenomenological with very little theoretical basis. These relations, however, are used as sub-models in computer codes for prediction of fuel cladding deformation under LOCA conditions. In the next subsection, we consider a phenomenological model for creep/superplasticity and in the subsequent section we delineate some engineering-type constitutive relations commonly used in computer codes for LOCA analysis.

3.1 Ashby-Verrall model

One of the principal attributes of crystal superplasticity is the action of *grain boundary sliding*. It refers to the displacement which takes place when, in response to an external stress, two grains slide over each other with the motion occurring at or in the close vicinity of their mutual interface. More precise definitions are given in [28]. The compatibility of a grain boundary in a polycrystalline material during grain boundary sliding is maintained by simultaneous accommodation processes which can involve grain boundary migration, grain rotation, diffusion and dislocation motion. The accommodation mechanisms may be separated into three parts, namely,

- accommodation by lattice diffusion and/or grain boundary diffusion,

[3] Superplasticity is the tendency of a polycrystalline to deform extensively at elevated temperatures ($T > 0.5T_m$), prior to rupture, where T_m is the melting point of the solid [26, 27].

- accommodation by dislocation motion, and
- combined effects of diffusion and dislocation motion.

Ashby and Verrall [29] described superplasticity as a transition region between the grain boundary diffusion, acting at low strain rates (low stresses), and dislocation creep operating at high strain rates. For grains to preserve compatibility during the deformation process, they undergo shape change and *accommodation strains* which allow (a group of) them to remain stuck together. This accommodation is achieved by diffusional transport of matter both by bulk diffusion through the grain and surface diffusion at grain boundaries. As the stress is raised, the diffusional accommodation strains are replaced by accommodation involving dislocation motion.
So these two mechanisms, the diffusional transport (low strain rate) and dislocation motion (high strain rate), characterize the structural and topological aspects of the superplastic flow. Moreover, at intermediate strain rates, these two mechanisms superimpose on each other. Because these two processes are assumed to be independent and occur concurrently, the total strain rate is taken as the sum of the strain rate of each contributor

$$\dot{\varepsilon}_{\mathrm{tot}} = \dot{\varepsilon}_{\mathrm{diff}} + \dot{\varepsilon}_{\mathrm{disc}}, \tag{2}$$

where the diffusional strain rate is [29]

$$\dot{\varepsilon}_{\mathrm{diff}} = 100\frac{\Omega D_{\mathrm{v}}}{k_B T d^2}\Big(\sigma - \frac{0.72\Gamma}{d}\Big)\Big(1 + \frac{3.3\delta}{d}\frac{D_{\mathrm{b}}}{D_{\mathrm{v}}}\Big), \tag{3}$$

and the dislocation strain rate is [29, 30]

$$\dot{\varepsilon}_{\mathrm{disc}} = \frac{A\mu}{k_B T}\Big(\frac{b}{d}\Big)^p\Big(\frac{\sigma}{\mu}\Big)^n \exp\Big(-\frac{Q_{\mathrm{d}}}{k_B T}\Big). \tag{4}$$

Here, $\dot{\varepsilon}$ is the strain rate (1/s), σ the tensile stress, Ω the atomic volume, d the grain size, Γ the grain boundary free energy, D_{v} the bulk diffusion coefficient, D_{b} the grain boundary diffusion coefficient, δ the thickness of the grain boundary, T the absolute temperature, k_B the Boltzmann constant, A is a material-dependent (dimensionless) constant, μ the shear modulus, b Burgers' vector, p an empirical inverse grain size exponent, $n = 1/m$ an empirical stress exponent, and Q_{d} the activation energy for deformation. Typical values for these parameters for Zircaloy-4 are presented in table 4. The theoretical bases for equations (3) and (4) are discussed in [29] and [30], respectively; and their detailed mathematical derivations are given in [31].
The Ashby-Verrall model is illustrated in figure 14, which shows a two-dimensional representation for a group of four hexagonal grains at strains of (a) $\varepsilon = 0$, (b) $\varepsilon = 0.275$, and (c) $\varepsilon = 0.55$, respectively. The model supposes that the grain change shape by diffusion to $\varepsilon = 0.275$, figure 15, when the central boundaries meet at a point. The point then splits to give two triple junctions and finally $\varepsilon = 0.55$. This type of grain boundary arrangement retains the equiaxed grains at high elongations without any grain growth. In situ observations in zinc-base alloys by high voltage electron microscopy seem to support this kind of behaviour [32]. Furthermore, observations and measurements on Zircaloy-4 at 1123 K and intermediate strain rates ($10^{-3} - 0.1\ \mathrm{s}^{-1}$) by Garde et al. [15] indicate that significant grain-boundary sliding is accompanied by minimal grain growth. The contribution of dislocation motion along grain boundaries as described by the Ashby & Verrall model is illustrated in figure 16.

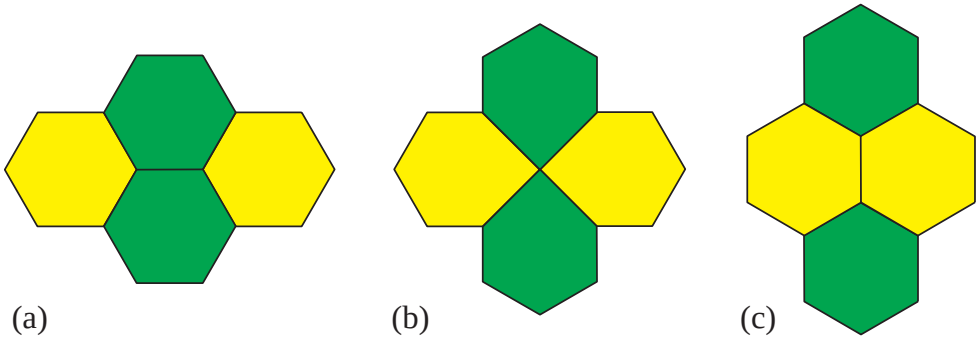

Figure 14: Schematic two-dimensional representation of superplastic deformation by grain rearrangement in a polycrystalline material according to the Ashby-Verrall model [29] at different strain levels (a) $\varepsilon = 0$, (b) $\varepsilon = 0.275$, and (c) $\varepsilon = 0.55$.

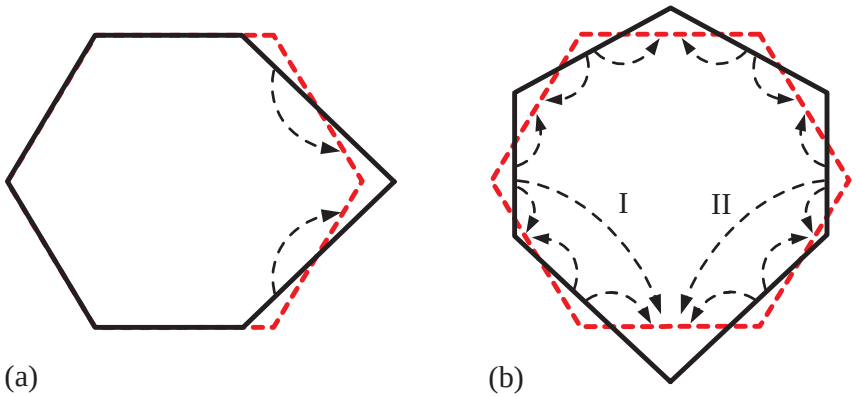

Figure 15: Schemata of diffusion paths associated with the grain rearrangement shown in figure 14 at $\varepsilon = 0.275$. The paths labeled I and II in (b) were not considered in the original model of Ashby and Verrall; after [33].

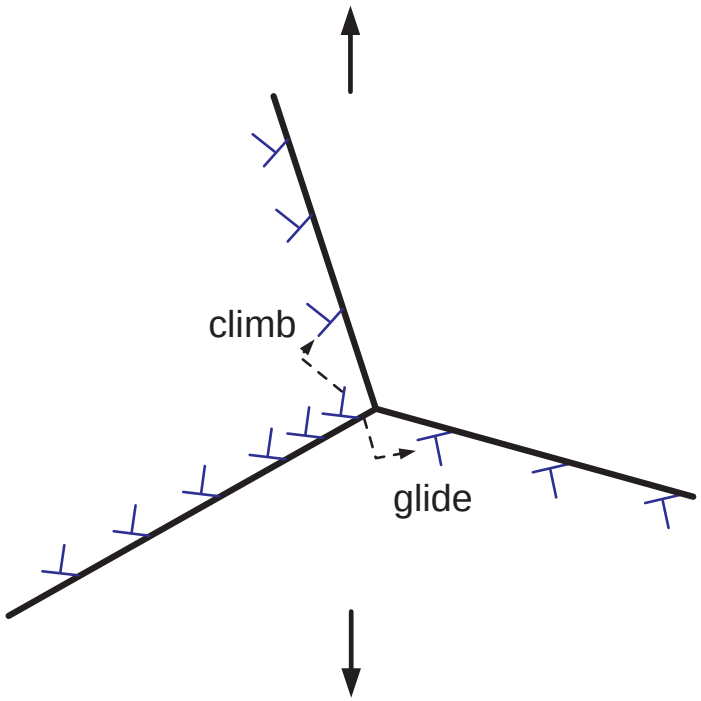

Figure 16: A schema of dislocation glide and climb along the grain boundaries of a polycrystalline according to the Ashby and Verrall model; after [33].

Table 4: Ashby-Verrall model parameter data for Zircaloy (Zry). Most of the data are from [15], except μ which is from [6], and $p = 1$, b, A are from [31]; here, T is temperature K.

Parameter		Units
Atomic volume	$\Omega = 2.37 \times 10^{-29}$	m^3
Bulk diffusion coefficient	$D_v = 5.9 \times 10^{-6} \exp(-218000/RT)$	m^2/s
Surface diffusion coefficient	$D_b = 5.9 \times 10^{-6} \exp(-130800/RT)$	m^2/s
Gas constant	$R = 8.3145$	J/(mol K)
Shear modulus (α-Zry)	$\mu = 2161T^2 - 2.36199 \times 10^7 T + 3.95472 \times 10^{10}$	Pa
Shear modulus (β-Zry)	$\mu = -1.893 \times 10^7 T + 4.026 \times 10^{10}$	Pa
Grain boundary energy	$\Gamma = 0$	J/m^2
Grain boundary thickness	$\delta = 1.0 \times 10^{-9}$	m
Burgers vector	$b = 3.3 - 5.0 \times 10^{-10}$ m	m
Stress exponent	$n = 4.35$	-
Grain size exponent	$p = 1$	-
Activation energy for creep	$Q_d = 316000$	J/mol
Creep strength constant (α-Zry)	$A = 1.0 \times 10^{-4}$	m^3/s
Creep strength constant (β-Zry)	$A = 1.0 \times 10^{-8}$	m^3/s

The application of the Ashby-Verrall model to a two-phase coexisting ($\alpha + \beta$) region was recently formulated in [31], where mixing rules for diffusivities and dislocation strain rates are employed. In this formulation, one writes equation (3) as

$$\dot{\varepsilon}_{\text{diff}}^{(\alpha+\beta)} = C_a \frac{\Omega}{k_B T d^2}\Big(\sigma - \frac{0.72\Gamma}{d}\Big)\Big(\bar{D}_{\text{V}} + \frac{\vartheta\delta}{d}\bar{D}_{\text{S}}\Big), \tag{5}$$

where

$$\bar{D}_{\text{X}} = D_{\text{X}\alpha}(1-y) + D_{\text{X}\beta}y, \tag{6}$$

X stands for V or S, $D_{\text{V}\alpha}$ denotes the volume self-diffusivity in the α-phase, y the volume fraction of the β-phase, and so forth. The dislocation induced creep rate in the two-phase domain equation (4) is expressed by

$$\dot{\varepsilon}_{\text{disc}}^{(\alpha+\beta)} = \frac{e^{-Q_{\text{d}}/k_B T}}{k_B T}\Big(\frac{b}{d}\Big)^p \Big[A_\alpha \mu_\alpha \Big(\frac{\sigma}{\mu_\alpha}\Big)^{n_\alpha}(1-y) + A_\beta \mu_\beta \Big(\frac{\sigma}{\mu_\beta}\Big)^{n_\beta} y\Big], \tag{7}$$

where μ_α is the shear modulus in the α-phase and so on. The volume fraction of the β-phase is calculated from an evolution equation for y dtailed in [31, 34, 35]. Finally, the total creep rate in the $(\alpha + \beta)$-domain is calculated according to (2): $\dot{\varepsilon}_{\text{tot}}^{(\alpha+\beta)} = \dot{\varepsilon}_{\text{diff}}^{(\alpha+\beta)} + \dot{\varepsilon}_{\text{disc}}^{(\alpha+\beta)}$. The values for the parameters in equations (6)-(7) for Zircaloy-4 and Zr1%Nb alloy are specified in table 1 of ref. [31].

3.2 Engineering type models

Two variants of empirical creep correlations for high temperature behaviour of Zircaloy and one variant for Zr1%Nb alloy are presented here. The correlations are designed for use in fuel rod safety analysis codes under LOCA conditions and are used here to evaluate the measured data presented in section 2.

3.2.1 Rosinger correlation

The steady-state creep strain rate of Zircaloy in single-phase (α domain or β domain) is expressed by a Norton law [36, 37]

$$\dot{\varepsilon}_\theta = A_\theta \exp(-Q/RT)\sigma_\theta^n, \tag{8}$$

where ε_θ and σ_θ are the hoop (tangential) strain and stress of the cladding tube, respectively, A_θ the strength coefficient, Q the activation energy, R the gas constant, T the absolute temperature, and n the stress exponent. The creep strength coefficient A_θ, as in ref. [37], is calculated from

$$A_\theta = \Big[\frac{1}{4}(F+G) + H\Big]^{(n-1)/2}(H + \frac{1}{2}F)(F+G)^{-(n+1)/2}A_z, \tag{9}$$

where the Hill anisotropic factors F, G and H [38] are used in the α-phase and isotropic values of $F = G = H = 0.5$ are used for the $(\alpha + \beta)$- and β-phase domains. For the anisotropic α-Zr alloy, we assume $F = 0.956$, $G = 0.304$ and $H = 0.240$ [36]. All the parameters appearing in equation (8) are specified in table 5 for Zircaloy-4. The strength coefficient A_θ for the Zr alloy is calculated from the corresponding uniaxial value A_z through the anisotropic factors by Hill's relation [36, 37, 39].

Table 5: Creep law parameters for Zircaloy-4 [37], cf. Eq. (8).

Parameter	Unit	α-phase	β-phase	$(\alpha+\beta)^*$
A_z	$\text{MPa}^{-n}\text{s}^{-1}$	19400	7.9	0.24
n	-	5.89	3.78	2.33
A_θ	$\text{MPa}^{-n}\text{s}^{-1}$	1489	3.97	0.15
Q/R	K	38487	17079	12316

* Valid for strain rates ≤ 0.003 1/s, otherwise linear interpolation of parameters between α and β phases are used.

Table 6: Creep constants for Eq. (10) determined by multiple regression analysis of Zircaloy-4 cladding data, from [6].

Phase domain	A_θ K(Pa s)^{-1}	A_z K(Pa s)^{-1}	n ...	Q kJ/mol
α	4.43×10^{16}	4.55×10^{17}	5.31 ± 0.06	266.8 ± 14.0
$(\alpha+\beta)^*$	3.63×10^{4}	5.50×10^{4}	1.89 ± 0.02	196.6 ± 10.0
β	1.49×10^{7}	2.92×10^{7}	3.68 ± 0.04	93.0 ± 5.0

* Values were obtained for $(\alpha+\beta)$ phase tube annealed for 600 s prior to deformation.

3.2.2 Donaldson correlation

Donaldson et al. [6] consider an empirical relation for the creep rate of Zircaloy-4 in the α phase and β phase range. The hoop strain rate as a function of temperature and hoop stress σ_θ is expressed as

$$\dot{\varepsilon}_\theta = A_\theta \frac{\mu}{T}\Big(\frac{\sigma_\theta}{\mu}\Big)^n \exp\Big(-\frac{Q}{RT}\Big). \tag{10}$$

where A_θ is a structure constant and other parameters were defined earlier. Note that equation (10) becomes equivalent to equation (4) when $p = 0$ in equation (4).
Donaldson et al. [6] fitted equation (10) to their measured creep data in the α phase and β phase range. They determined the parameters A_θ, n and Q using a multiple regression analysis for which the best fit values and uncertainties are given in table 6. Note that the values for A_z are calculated through equation (9) as before.
For the $(\alpha+\beta)$ mixed phase range, i.e. temperatures between about 1073 to 1173 K, within a narrow range of strain rates of the order of 10^{-4} s^{-1}, creep in Zircaloy occurs by superplastic flow. As alluded earlier, superplastic behaviour is caused by grain boundary sliding and grain switching with the outcome that the observed creep rate varies inversely with grain size, cf. equation (4). Moreover, it has been observed that at intermediate strain rates (10^{-4}-10^{-3} s^{-1}) grain growth is insignificant while grain boundary sliding is prevailing [15]. For the tested specimens annealed for 600 s prior to creep testing, it was assumed that the grain growth during creep deformation was negligible in the temperature range of 1123 to 1173 K and strain rates between 4×10^{-5} and 2×10^{-3} s^{-1}. Thus the creep rate equation (10) was fitted to the data by means of a multiple regression analysis, with best-fit constants given in table 6.

Table 7: Creep law parameters for Zircaloy-4 alloy [7], cf. Eq. (11).

Parameter	Unit	α-phase ($\sigma \leq 15$ MPa)	α-phase ($\sigma > 15$ MPa)
A_z	KMPa^{-n}s^{-1}	1.00×10^6	1.63×10^8
n	-	1.3	5.0
A_θ	KMPa^{-n}s^{-1}	5.04×10^5	1.80×10^7
Q/R	K	22852	38006
		β-phase	$(\alpha+\beta)$-phase
A_z	KMPa^{-n}s^{-1}	1.00×10^4	NA
n	-	4.25	1.3
A_θ	MPa^{-n}s^{-1}	4.70×10^3	NA
Q/R	K	18041	NA

3.2.3 Kaddour correlation

Kaddour et al. [7] used a Harper-Dorn law [40] to describe the steady-state creep strain rate of both Zircaloy-4 and Zr1%Nb alloy in single-phase (α domain or β domain), namely

$$\dot{\varepsilon}_\theta = \frac{A_\theta}{T} \exp(-Q/RT)\sigma_\theta^n, \tag{11}$$

Recall that Kaddour et al. [7] carried out their creep tests in the axial direction; so in writing equation (11), we have tacitly used equation (9), as before, to express $\dot{\varepsilon}_\theta$ in terms of A_θ and σ_θ. All the parameters appearing in equation (11) are described in tables 7 and 8 for Zircaloy-4 and Zr1%Nb alloy, respectively. Kaddour et al. [7] note that in the α-phase their results show two creep mechanisms: At low stresses ($\sigma < 15$ MPa), the deformation could be due to diffusion creep ($n \approx 1$), while at higher stresses ($\sigma > 15$ MPa) it is most probably dislocation creep ($n \approx 4$) which is operating, cf. tables 7-8. In the β-phase, the investigators only found one mechanism, i.e. dislocation creep. They point out that the creep behaviour for both Zircaloy-4 and Zr1%Nb in the $(\alpha+\beta)$ domain is more complex than in single phase domains. They could not identify a simple constitutive equation, which would describe the creep rate for this regime. They suggest that in this domain the creep deformation mechanism could be controlled by inter-phase interface sliding for which apparently no theoretical description (accounting for the dependence on stress and temperature) exists. The strain rate in the two-phase coexistence ($\alpha+\beta$) region follows a separate mechanism than in the single phase region [5, 23]. For computational convenience, some authors have suggested ad-hoc correlations in the mixed-phase region for Zircaloy-4 [36, 37] or have considered homogenization according to [41, 42]

$$\dot{\varepsilon}_{\alpha\beta} = \dot{\varepsilon}_\alpha(1-y) + \dot{\varepsilon}_\beta y\,, \tag{12}$$

or alternatively

$$\dot{\varepsilon}_{\alpha\beta} = \dot{\varepsilon}_\alpha^{1-y} \cdot \dot{\varepsilon}_\beta^{y}\,, \tag{13}$$

where subscripts α and β refer to the respective phases, and y is the volume fraction of the β phase calculated from a phase transformation model, e.g. [34, 35].

Table 8: Creep law parameters for Zr1%Nb alloy [7], cf. Eq. (11).

Parameter	Unit	α-phase ($\sigma \leq 15$ MPa)	α-phase ($\sigma > 15$ MPa)
A_z	MPa^{-n}s^{-1}	6780	2280
n	-	1.0	4.0
A_θ	MPa^{-n}s^{-1}	3864	380
Q/R	K	15996	23333
		β-phase	$(\alpha+\beta)$-phase
A_z	MPa^{-n}s^{-1}	1230	NA
n	-	4.3	1.4
A_θ	MPa^{-n}s^{-1}	574	NA
Q/R	K	17079	NA

* NA = not available.

4 Evaluation of creep rate

In this section, we evaluate the creep data presented in section 2 using the constitutive relations delineated in section 3. Our input to the equations are test temperature and applied stress, while the output is the creep rate versus applied stress at different temperatures for each set of data. The relative difference between model calculations and measurements are quantified. More specifically, the average relative difference in creep rate between the calculated and measured value in a data set is defined by

$$\langle \mathrm{R}_n \rangle = \frac{1}{n} \sum_{i=1}^{n} \frac{|\mathrm{M}_i - \mathrm{C}_i|}{\mathrm{M}_i}. \tag{14}$$

where M_i and C_i are the i-th measured and calculated creep rate, respectively, and n is the number of measurements in the data set. Note that the equations in section 3 used to calculate the creep rate were qualified or verified with different portions of the data summarized in section 2 as detailed in the literature.
For example, Eq. (8) and its associating constants were verified by Rosinger et al. [5] with uniaxial tensile creep data on Zircaloy-4 samples, see subsection 2.1.1, whereas Eq. (10) and its constants were obtained by Donaldson et al. [6] using regression analysis on biaxial tensile creep data, see subsection 2.1.2. In this section, we will use both these equations to evaluate all the considered Zircaloy-4 data. Regarding creep of Zr1%Nb, we will use Eq. (11) and its associated constants, obtained by Kaddour et al. [7] from uniaxial creep data, to the single phase domains of the alloy, while employing equations in section 3.1 to calculate the creep rate in the coexisting $(\alpha + \beta)$-phase, as were obtained in [31]. The operation carried out by Eq. (14) is for the final control or comparison, where we have selected the L_1-norm for simplicity. The results of our evaluations of the (creep rate) data are presented in a number of figures and the table below.

4.1 Zircaloy-4 α domain

We use equations (8) and (10) in the α domain to calculate the creep rate for the aforementioned tests. Figures 17 and 18 compare the results of our calculations and the data presented in figure 4, see also table 1. Figure 19 presents measured versus calculated values for the creep rate data shown in figures 17 and 18. The average relative difference between the measured and calculated values ($\langle \mathrm{R}_n \rangle$) for this set of data are given in table 9; data set 1. Figures 20 and 21 show the corresponding plots for the data by Donaldson et al. [18] presented earlier in figure 8, with $\langle \mathrm{R}_n \rangle$ values given in table 9; data set 2.

4.2 Zircaloy-4 ($\alpha + \beta$) domain

The evaluations are made by using equations (8) and (10) applicable in the $(\alpha + \beta)$ domain in Zircaloy-4. We should mention that in invoking equation (8) and the associating table 5, we have opted to use the $(\alpha + \beta)$ values given in the table for all the strain rates, that is, we have not switched to a different set of values (interpolated values) for the strain rates > 0.003 s^{-1}, as will be motivated in section 5.
Figure 22 compares the results of creep rate calculations and measurements for the Zircaloy-4 data displayed in figure 5 and specified in table 2. Figure 23 depicts measured versus calculated values of the creep strain rate for this data set. Figures 24 and 25 show the corresponding plots for the data displayed in figure 9 [17]. The average relative difference

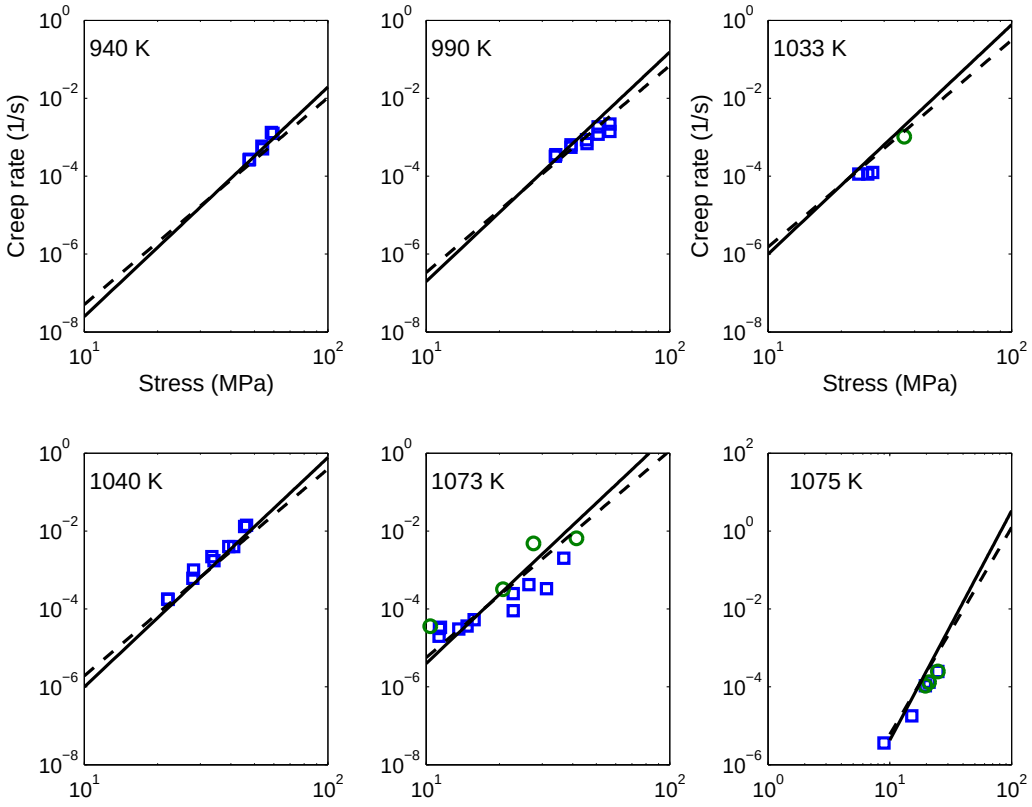

Figure 17: Axial creep strain rate versus nominal axial stress in the Zircaloy-4 α domain, cf. figure 4 and table 1. Symbols are measured values, the solid line is the output of Eq. (8) and the dashed line that of Eq. (10).

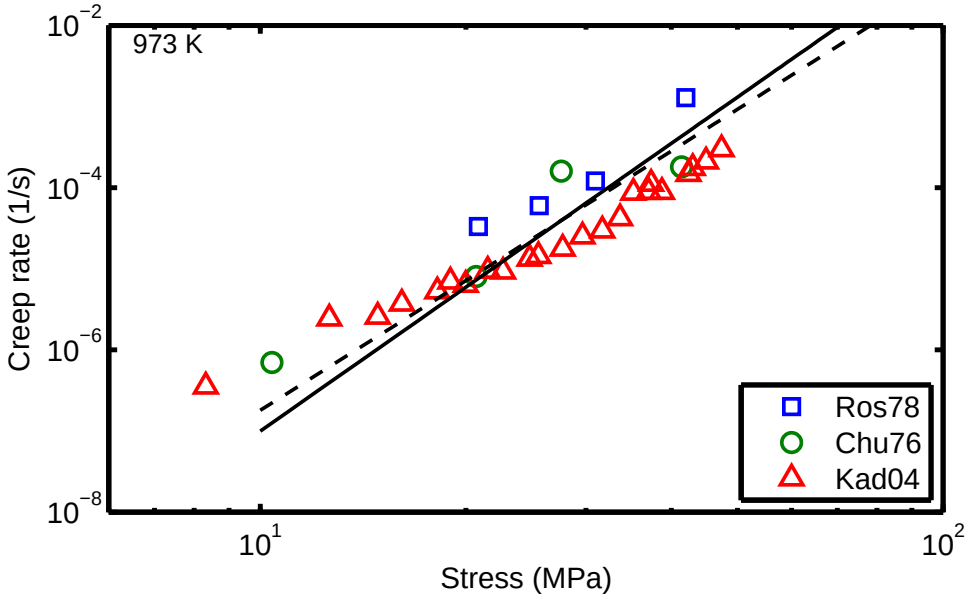

Figure 18: Axial creep strain rate versus nominal axial stress in the Zircaloy-4 α domain, cf. figure 4 and table 1. Symbols are measured values, the solid line is the output of Eq. (8) and the dashed line that of Eq. (10). Here Ros78: AECL data in [8], Chu76: Chung et al. data in [8] and Kad04: [7].

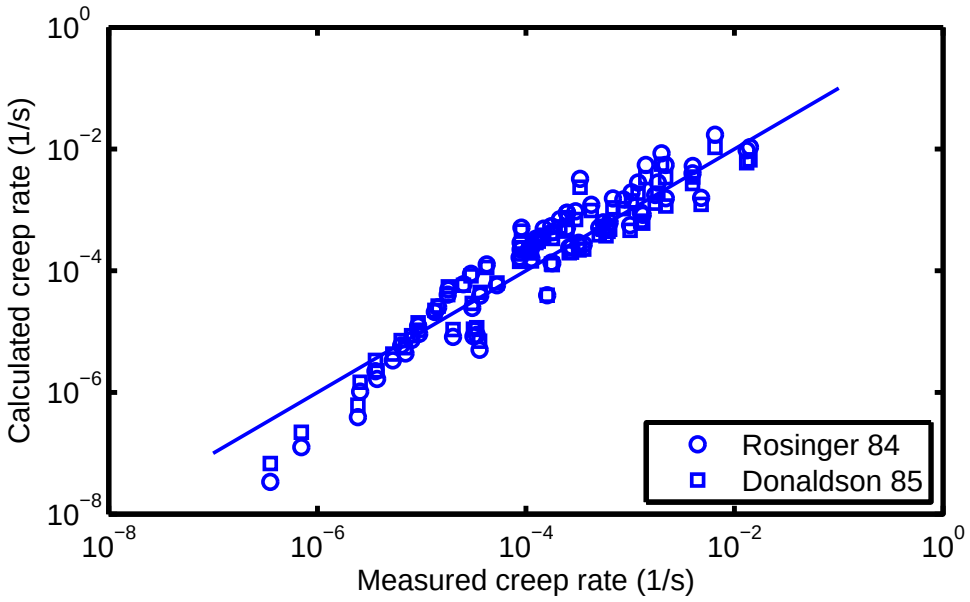

Figure 19: Measured versus calculated axial creep strain rate in the Zircaloy-4 α domain, cf. figures 17-18. Rosinger 84 is the output of Eq. (8) and Donaldson 85 that of Eq. (10).

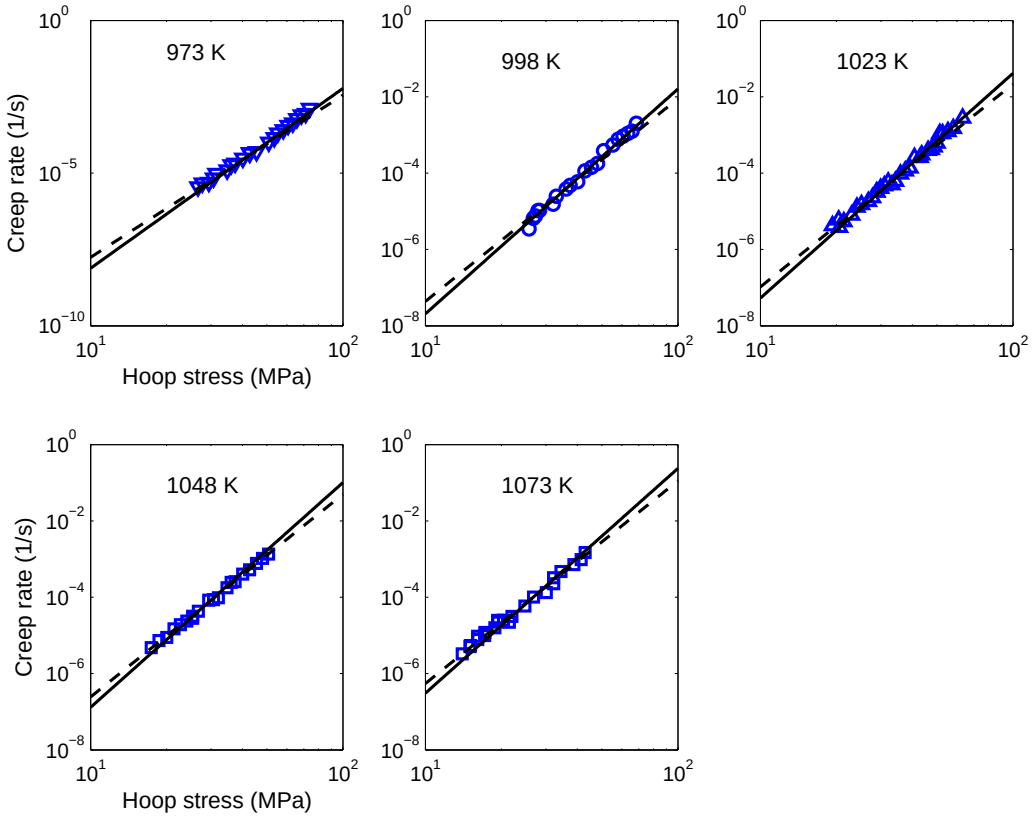

Figure 20: Hoop creep strain rate versus hoop stress in the Zircaloy-4 α domain, cf. figure 8. Symbols are measured values, the solid line is the output of Eq. (8) and the dashed line that of Eq. (10).

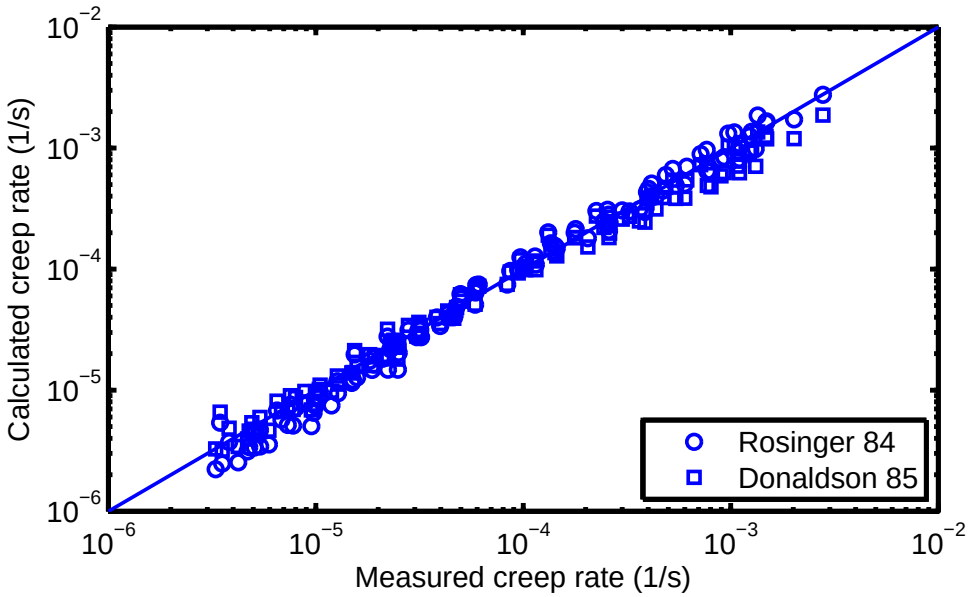

Figure 21: Measured versus calculated hoop creep strain rate in the Zircaloy-4 α domain, cf. figures 8 and 20. Rosinger 84 is the output of Eq. (8) and Donaldson 85 is that of Eq. (10).

between the measured and calculated values, $\langle \mathrm{R}_n \rangle$, for the associating figures 23 and 25 are given in table 9, data sets 3 and 4, respectively.

4.3 Zircaloy-4 β domain

The evaluation of creep rate for the Zircaloy-4 β domain are made using equations (8) and (10), and the parameter values in tables 5 and 6, respectively.
We first consider the data displayed in figure 6a, namely, AECL's own data [8]. Figures 26 and 27 compare the results of creep rate calculations and measurements. Figure 28 shows the measured versus calculated values of the creep strain rate for this data set. The average relative difference between the measured and calculated values, $\langle \mathrm{R}_n \rangle$, associated with figure 28, are given in table 9; data set 5.
Other workers' data presented in [8] plus the data at 1273 K [7], cf. figure 6b and table 3, are evaluated in figures 29 and 30. The corresponding $\langle \mathrm{R}_n \rangle$ values are given in table 9; data set 6.
The results of the evaluations of the Zircaloy-4 β domain data in [6] are presented in figures 31-32 and table 9; data set 7.

4.4 Zr1%Nb β domain

For the Zr1%Nb creep tests, we first evaluate the β domain data. Figure 33 depicts creep rate as a function of applied stress at temperatures from 1233 K to 1373 K, for both measured and calculated values. Calculations were done by using equation (11) and the associating table 8 for β-phase. Figure 34 shows measured versus calculated values. The one-to-one correlation is up to par with a small $\langle \mathrm{R}_n \rangle$; table 9, data set 8.

Table 9: The average relative difference between measured and calculated creep strain rate $\langle \mathrm{R}_n \rangle$, cf. Eq. (14), of the data base.

Data set	Figure no.	No. of measurements	$\langle \mathrm{R}_n \rangle$	$\langle \mathrm{R}_n \rangle$
...	...	...	Eq. (8)	Eq. (10)
		α-Zircaloy-4		
1	19	$n = 80$	1.05	0.913
2	21	$n = 115$	0.173	0.155
		$(\alpha + \beta)$-Zircaloy-4		
3	23	$n = 60$	1.196	0.631
4	25	$n = 106$	1.787	0.962
		β-Zircaloy-4		
5	28	$n = 37$	0.310	0.363
6	30	$n = 102$	0.607	1.207
7	32	$n = 102$	0.227	0.116
		β-Zr1%Nb		
...	...	...	Eq. (11)	...
8	34	$n = 16$	0.203	...
		$(\alpha + \beta)$-Zr1%Nb		
...	...	...	Eq. (2)	...
9	37	$n = 39$	0.382	...
		α-Zr1%Nb		
...	...	...	Eq. (11)	...
10	38b	$n = 55$	0.156	...

4.5 Zr1%Nb ($\alpha + \beta$) domain

For Zr1%Nb alloy (and Zircaloy-4) no simple constitutive equation was identified in [7]. Therefore we have attempted to employ the Ashby-Verrall model for diffusion-controlled creep and superplasticity, delineated in section 3.1 and in [31], to evaluate the creep data in the two-phase coexisting ($\alpha + \beta$) domain.
First, we expand the data set presented in figure 13 in the ($\alpha + \beta$) domain to higher stresses, by including additional data made available in D. Kaddour's doctoral dissertation [43], see figure 35. The results of creep rate calculations and measurements as a function of stress at various temperatures are presented in figure 36. The calculations are made by using the Ashby-Verrall relations (6)-(7), (4), and Table 1 in [31]. Figure 37 shows the measured versus calculated values of the creep strain rate for this data set. The average relative difference between the measured and calculated values, $\langle \mathrm{R}_n \rangle$, associated with figure 37, is given in table 9; data set 9. Details of the calculational method are described in [31].

4.6 Zr1%Nb α domain

Finally, the creep rate data for Zr1%Nb in the α domain is considered here. Figure 38a depicts creep rate as a function of applied stress at temperatures from 923 to 1033 K, for both measured and calculated values. Calculations were done by using equation (11) and the associating table 8 for α-phase. Figure 38b shows measured versus calculated values. The one-to-one correlation is excellent with a small $\langle \mathrm{R}_n \rangle$; table 9, data set 10.

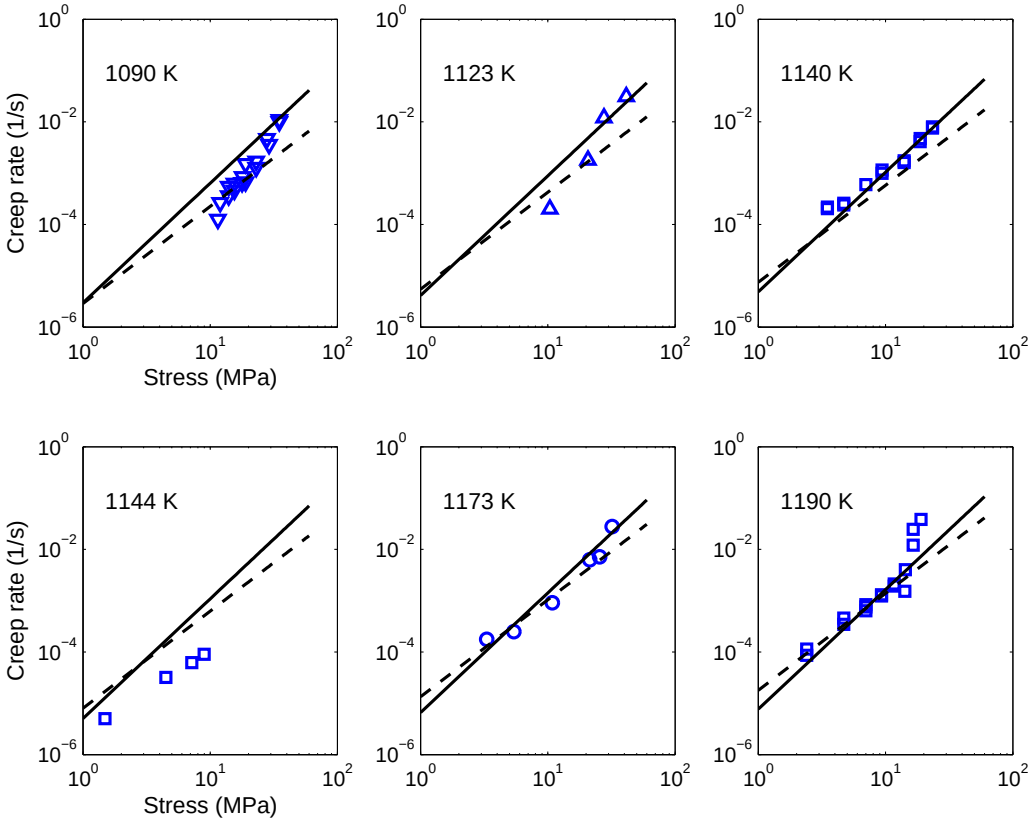

Figure 22: Axial creep strain rate versus nominal axial stress in the Zircaloy-4 ($\alpha + \beta$) domain, cf. figure 5. Symbols are measured values, the solid line is the output of Eq. (8) and the dashed line that of Eq. (10).

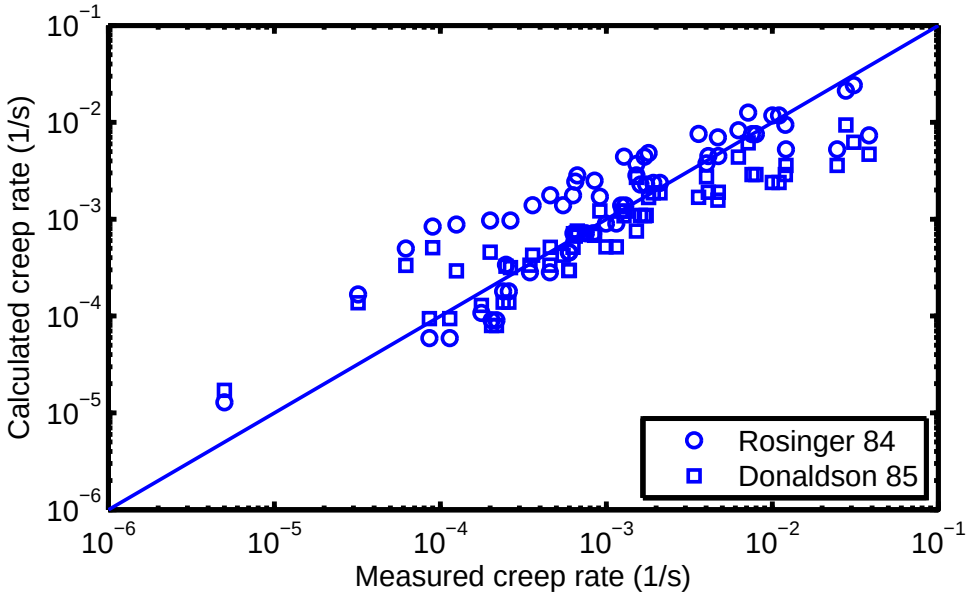

Figure 23: Measured versus calculated axial creep strain rate in the Zircaloy-4 ($\alpha + \beta$) domain, cf. figure 22. Rosinger 84 is the output of Eq. (8) and Donaldson 85, Eq. (10).

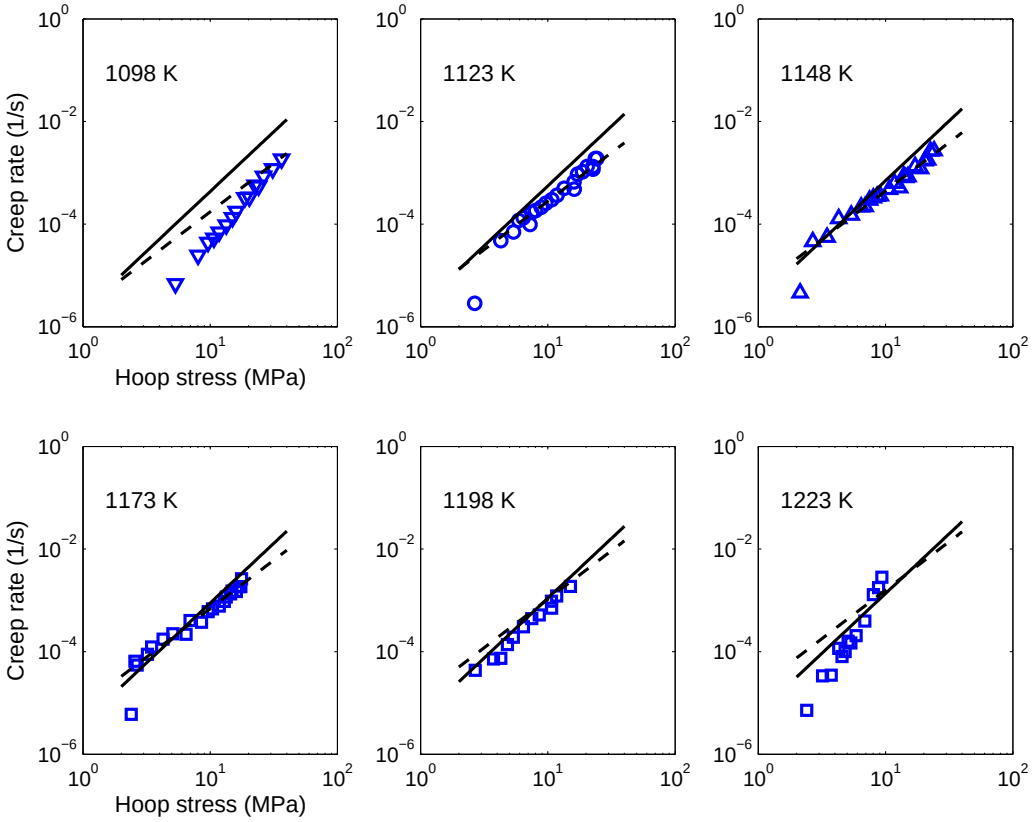

Figure 24: Creep hoop strain rate versus hoop stress in the Zircaloy-4 ($\alpha + \beta$) domain, cf. figure 9 and [17]. Symbols denote measured values, the solid line is the output of Eq. (8) and the dashed line that of Eq. (10).

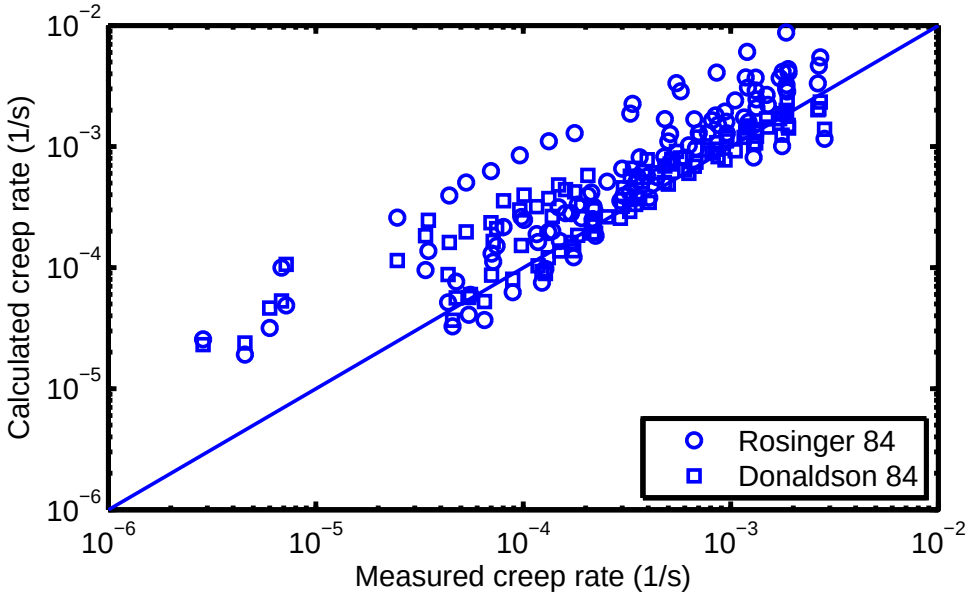

Figure 25: Measured versus calculated creep hoop strain rate in the Zircaloy-4 ($\alpha + \beta$) domain, cf. figure 24. Rosinger 84 is the output of Eq. (8) and Donaldson 85 is that of Eq. (10).

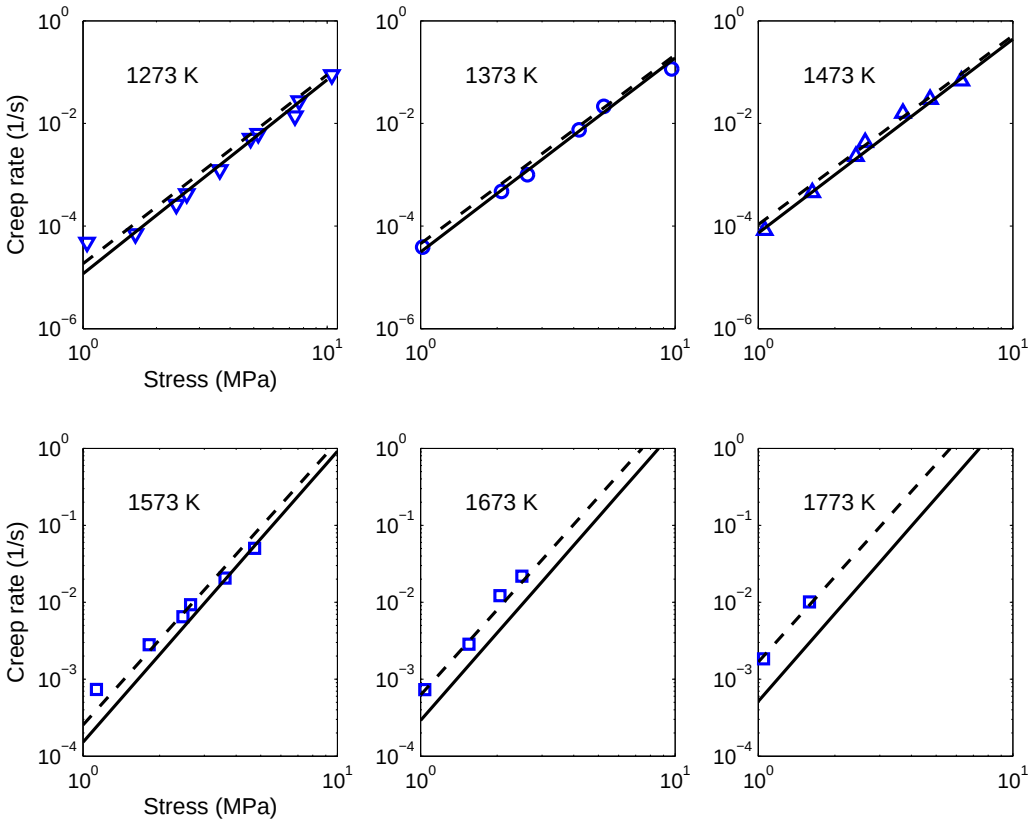

Figure 26: Axial creep strain rate versus nominal axial stress in the Zircaloy-4 β domain, cf. figure 6a. Symbols are measured values, the solid line is the output of Eq. (8) and the dashed line is that of Eq. (10).

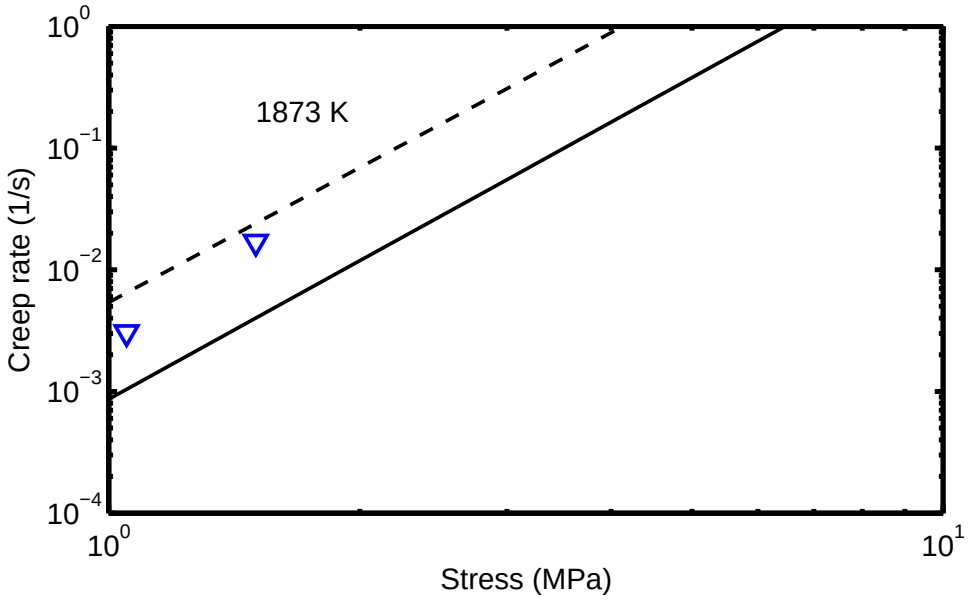

Figure 27: Axial creep strain rate versus nominal axial stress in the Zircaloy-4 β domain, cf. figure 6a. The triangles are measured values, the solid line is the output of Eq. (8) and the dashed line is that of Eq. (10).

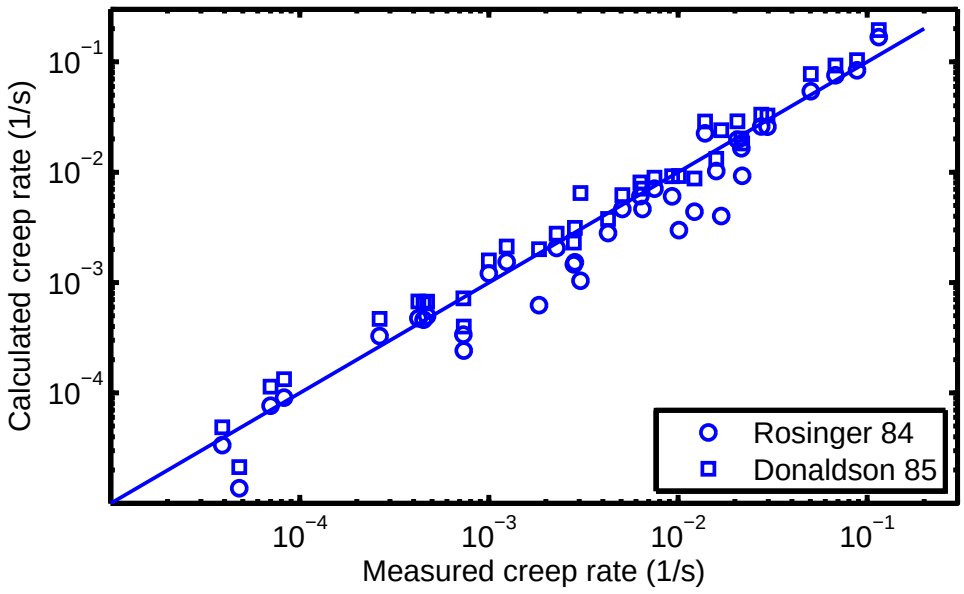

Figure 28: Measured versus calculated axial creep strain rate in the Zircaloy-4 β domain, cf. figures 26 and 27. Rosinger 84 is the output of Eq. (8) and Donaldson 85, Eq. (10).

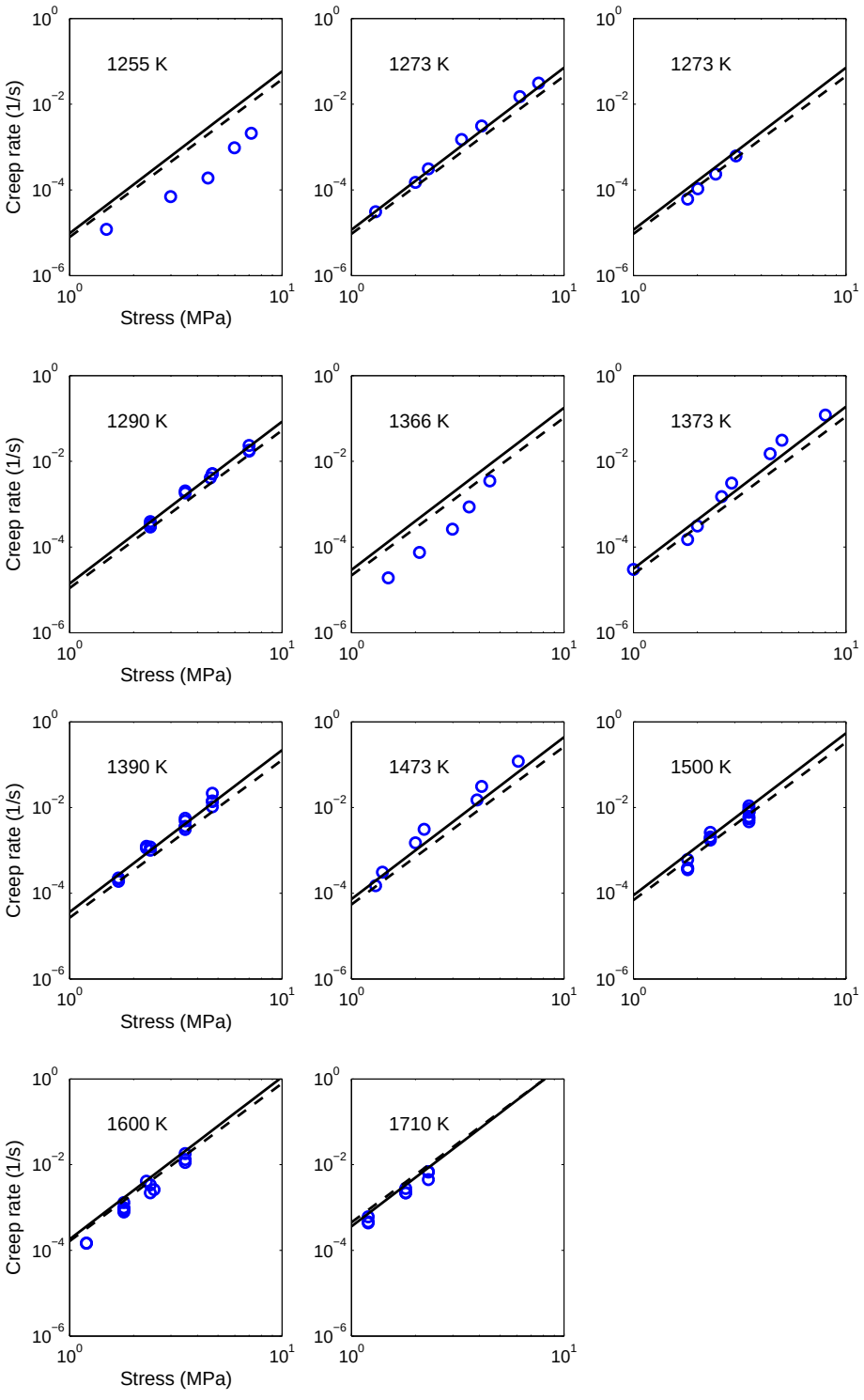

Figure 29: Axial creep strain rate versus nominal axial stress in the Zircaloy-4 β domain, cf. figure 6b and table 3, i.e., other workers' data presented in [8] plus the data at 1273 K [7]. Circles are the measured values, the solid line is the output of Eq. (8) and the dashed line is that of Eq. (10).

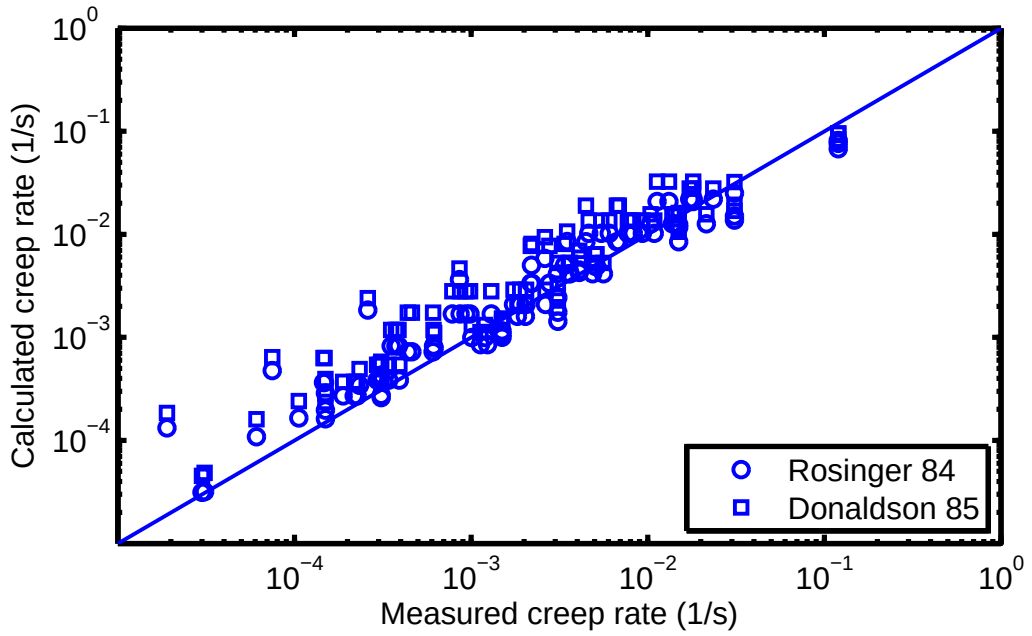

Figure 30: Measured versus calculated axial creep strain rate in the Zircaloy-4 β domain, cf. figure 29. Rosinger 84 is the output of Eq. (8) and Donaldson 85 that of Eq. (10).

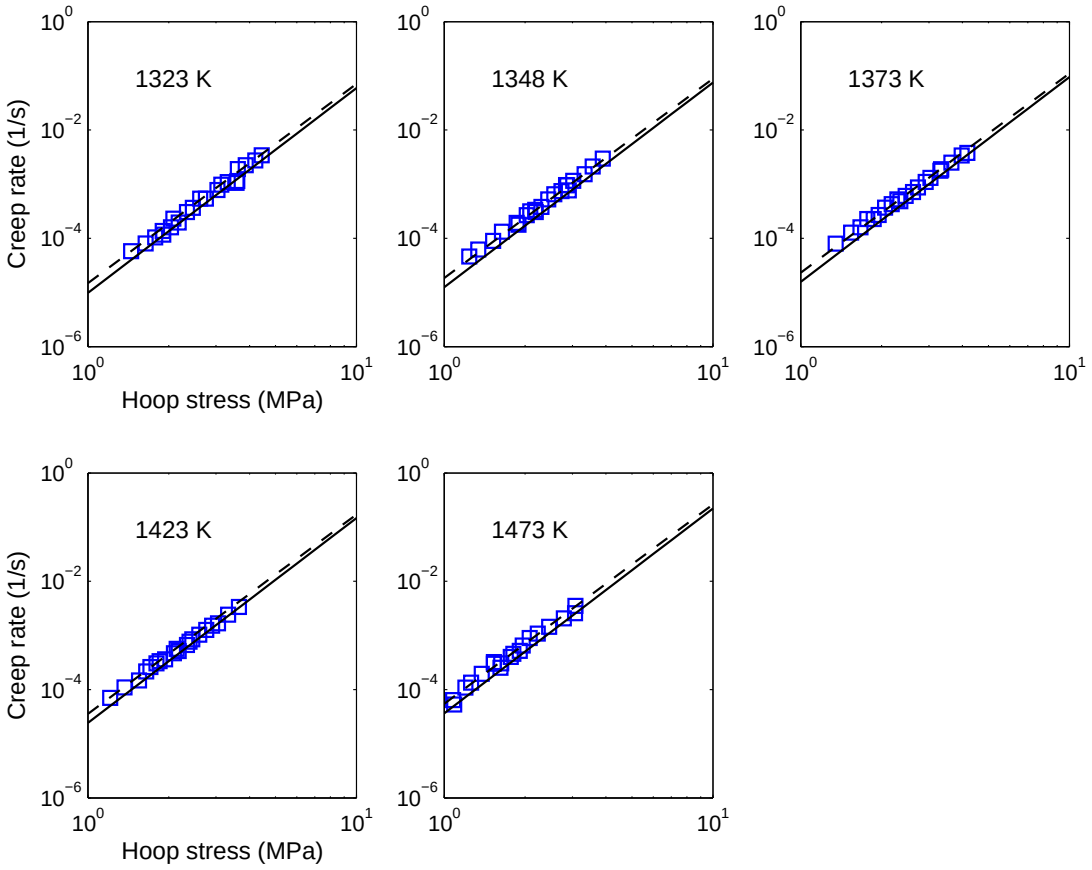

Figure 31: Hoop creep strain rate versus hoop stress in the Zircaloy-4 β domain, cf. figure 10 based on the data in [6]. Squares are the measured values, the solid line is the output of Eq. (8) and the dashed line is that of Eq. (10).

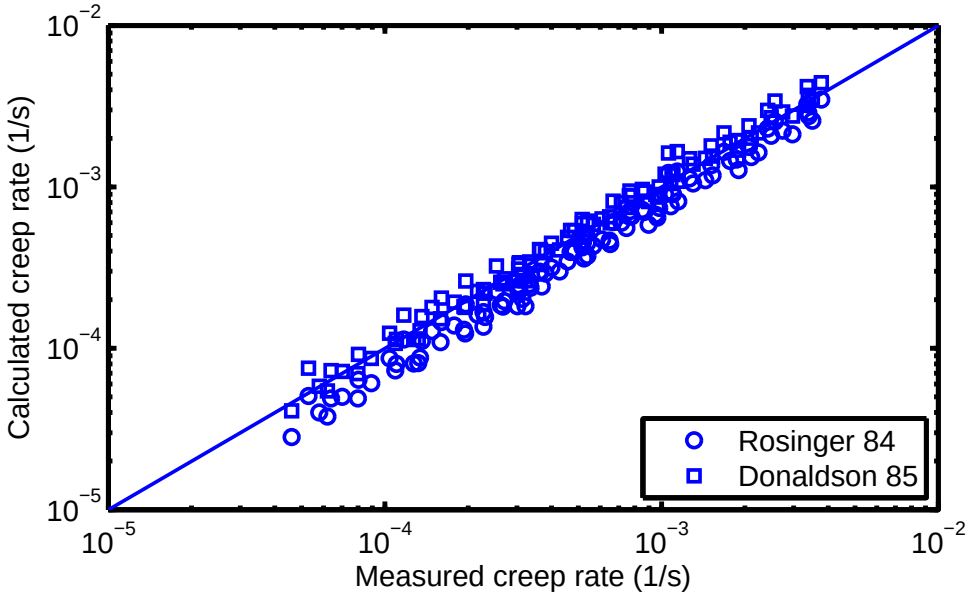

Figure 32: Measured versus calculated creep hoop strain rate in the Zircaloy-4 β domain, cf. figure 31. Rosinger 84 is the output of Eq. (8) and Donaldson 85 that of Eq. (10).

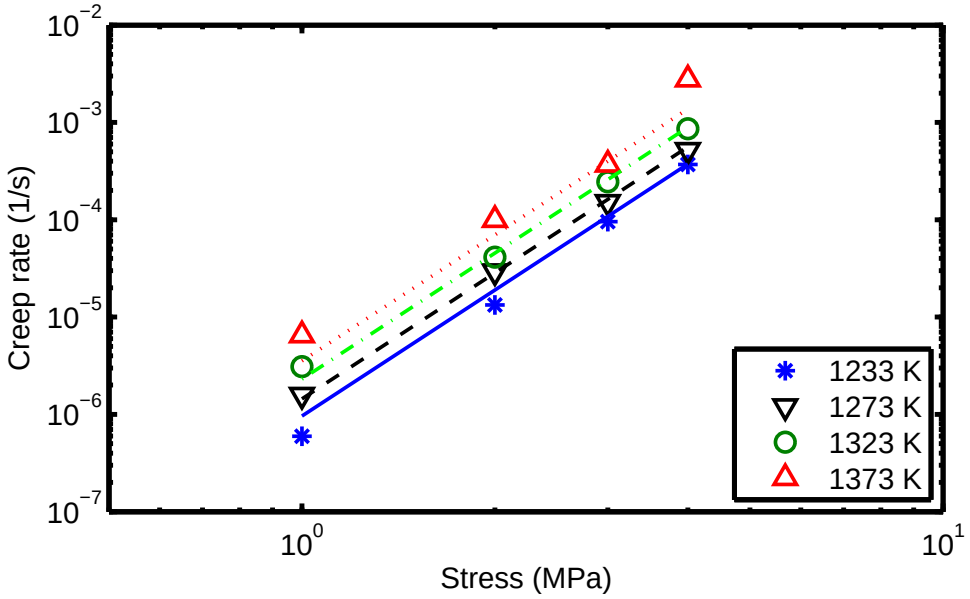

Figure 33: Axial creep strain rate versus nominal axial stress in the Zr1%Nb β domain based on the data in [7]. Symbols are the measured values and lines are the output of Eq. (11).

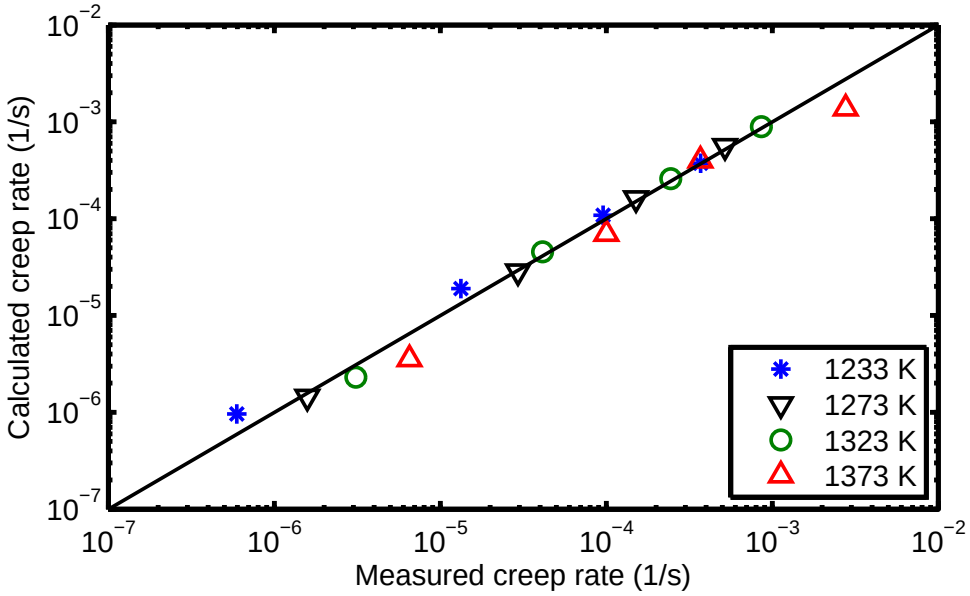

Figure 34: Measured versus calculated creep axial strain rate in the Zr1%Nb β domain, cf. figure 33.

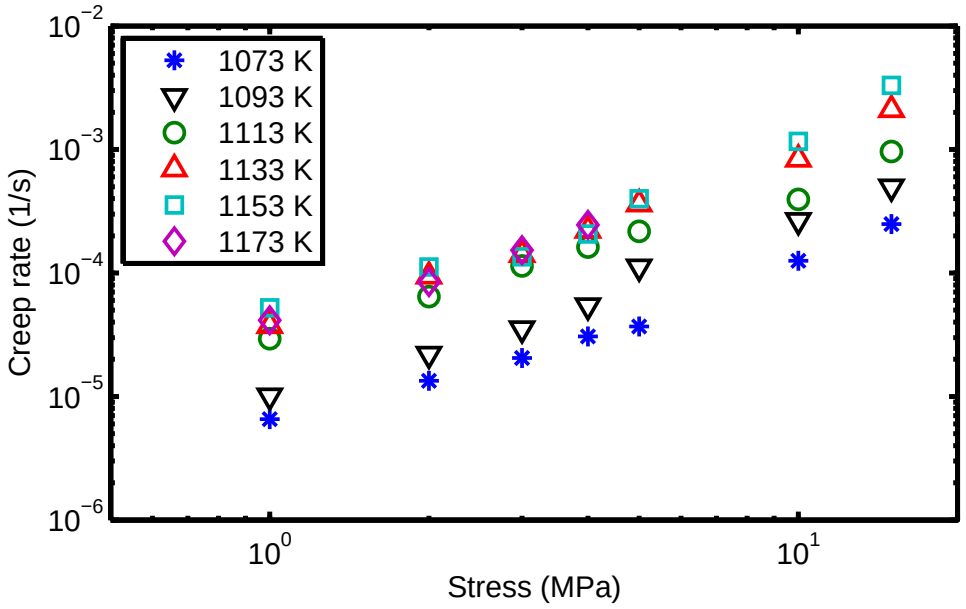

Figure 35: Measured true axial strain rate versus axial stress in the $(\alpha + \beta)$ domain of Zr1%Nb alloy at different temperatures, from [7, 43].

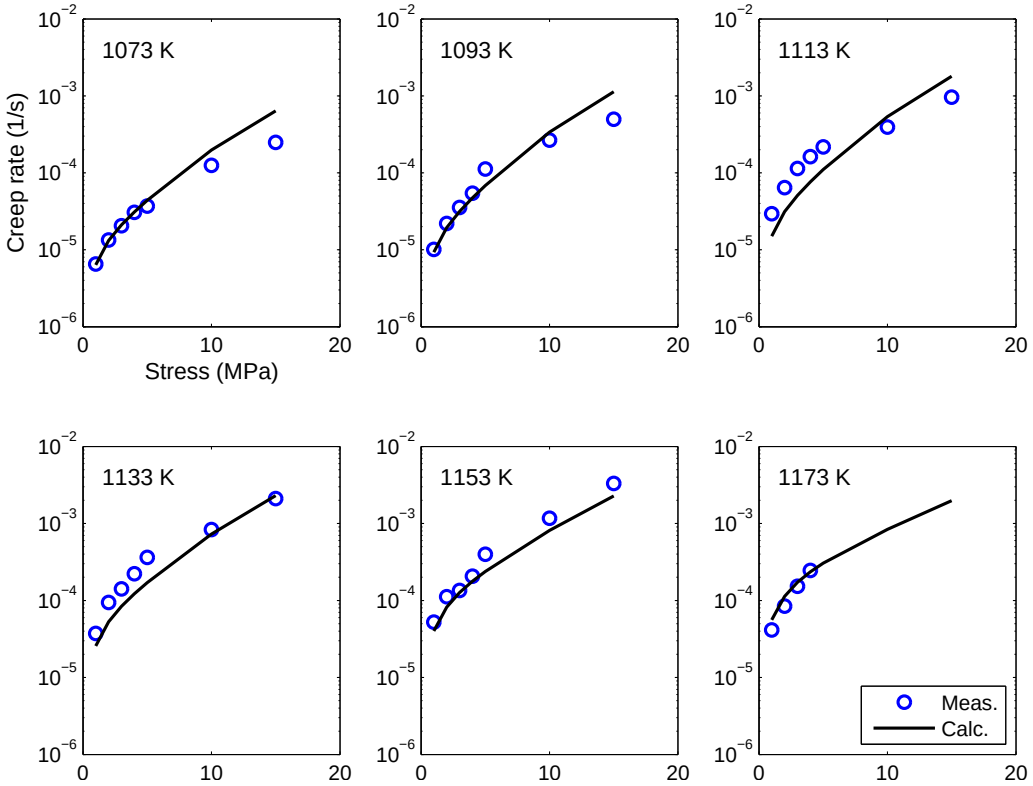

Figure 36: Axial creep strain rate versus axial stress in the Zr1%Nb $(\alpha + \beta)$ domain based on the data in [7, 43], cf. figure 35. Circles are the measured values and lines are the output of Eqs. (6)+(7); see [31].

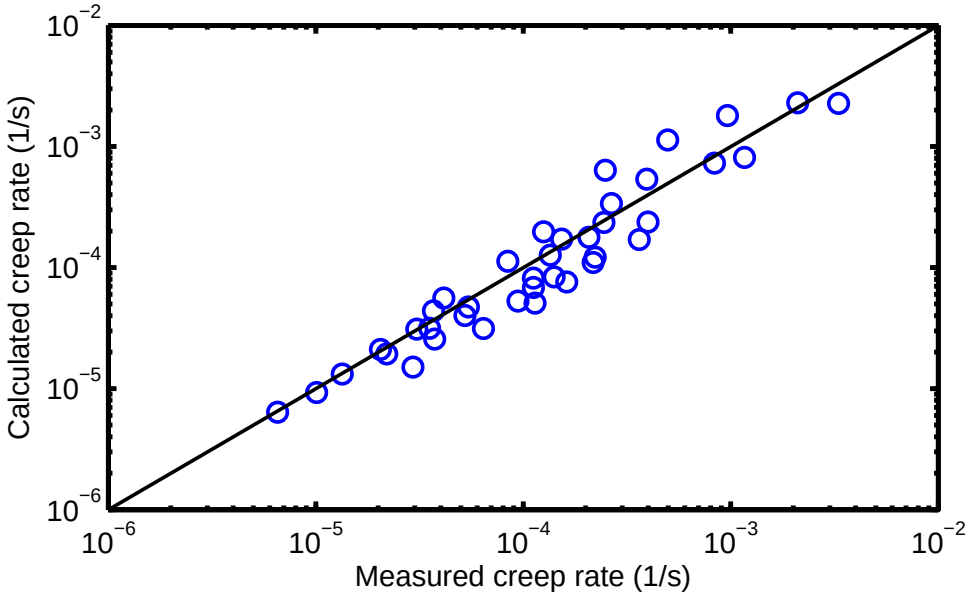

Figure 37: Measured versus calculated creep axial strain rate in the Zr1%Nb ($\alpha+\beta$) domain, cf. figure 36: from [31].

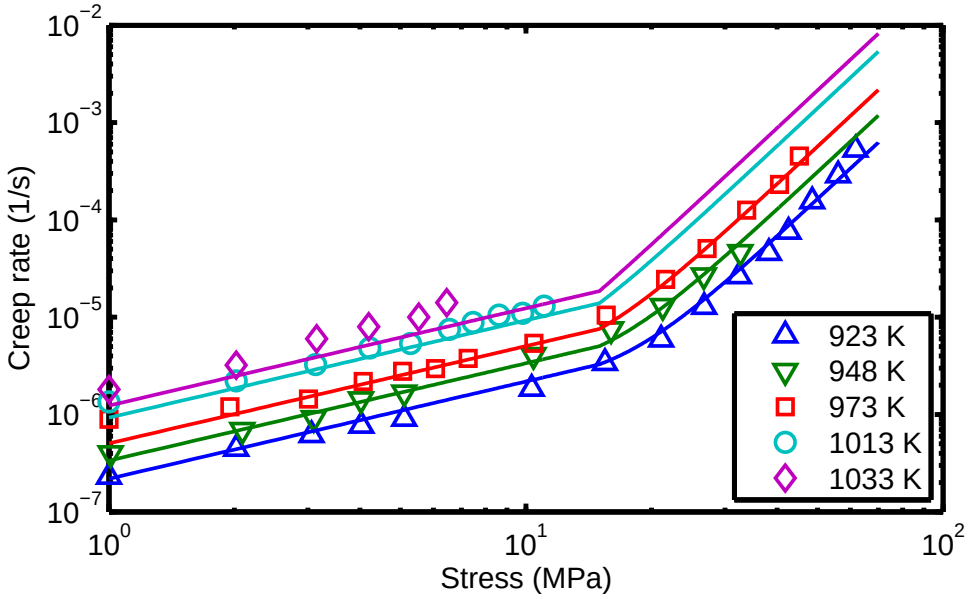

(a)

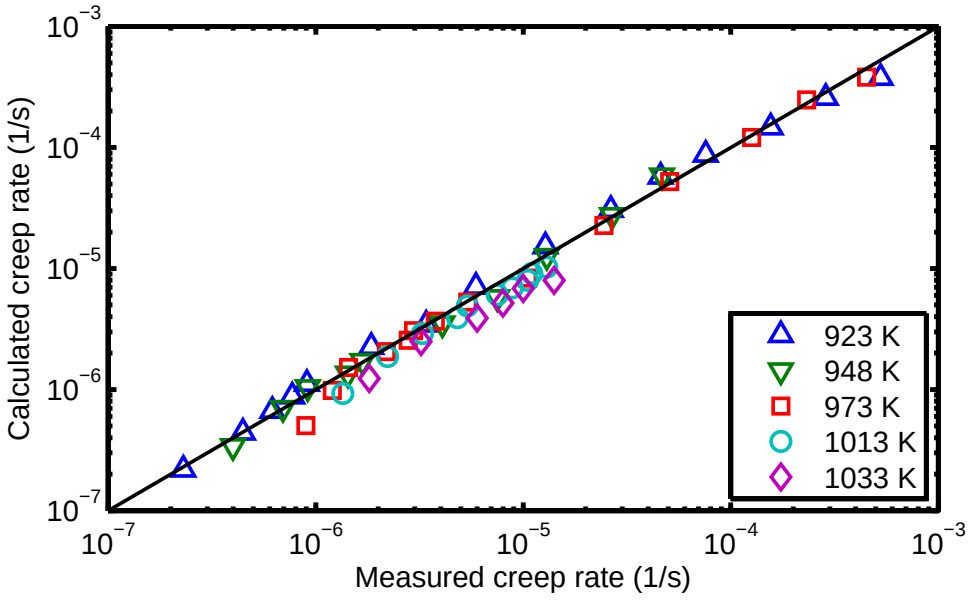

(b)

Figure 38: (a) Axial creep strain rate versus axial stress in the Zr1%Nb α domain based on the data in [7, 43]. Circles are the measured values and lines are the output of Eq. (11). (b) Measured versus calculated creep axial strain rate.

5 Discussion

The evaluation of test data in the foregoing section using the equations outlined in section 3.2 indicates that the engineering type constitutive relations capture the creep rate data in the single-phase β domain satisfactorily. In the two-phase coexisting $(\alpha + \beta)$ domain, however, the outcome is different. Firstly, despite an ad hoc fitting of the Zircaloy-4 creep rate equation to measured data resulting in a different set of model parameter values in the $(\alpha + \beta)$ domain -cf. equation (8) and table 5- the capability of the model to capture the data is rather poor, see table 9. Secondly, the arbitrary condition imposed on the equation, without providing the physical motivation or explanation, restricts its usage.

For example, in applying equation (8), the choice of model parameters depends on the strain rate. The parameter values listed in table 5 for the $(\alpha + \beta)$ domain are stated to be valid for strain rates ≤ 0.003 1/s, otherwise, linear interpolation of parameters between α and β phases is recommended. Our evaluation of the $(\alpha + \beta)$ creep data showed that this constraint on the creep rate does not improve the value of the relative difference between measured and calculated values, and hence, we do not recommend it. Also, in the usage of equation (10) in the $(\alpha + \beta)$ domain of Zircaloy-4, the parameter values listed in table 6 were determined for tubes which were annealed for ten minutes at test temperatures prior to pressurizing and carrying out the creep test [6]. Since annealing can have an impact on creep behaviour, the applicability of these values to other Zircaloy-4 materials with different as-received heat treatments is questionable. Nevertheless, as can seen from table 9, Donaldson et al.'s correlation, equation (10), is in better agreement with the Zircaloy-4 experimental data in the $(\alpha + \beta)$ domain than that of Rosinger and co., i.e. equation (8). Therefore, Donaldson et al.'s correlation should be utilized in this domain for Zircaloy-4.

As mentioned in section 3.2.3, in the β domain of both Zircaloy and Zr1%Nb alloy, Kaddour et al. [7] observed only one mechanism for secondary creep, namely, "dislocation climb induced creep", cf. equation (11) and tables 7-8. In the two-phase coexistence $(\alpha+\beta)$ domain, Kaddour et al. [7] could not identify any constitutive relation for creep of the two alloys, however, they observed that at very low applied stresses (1-2 MPa), strain rates in the $(\alpha + \beta)$ domain are substantially higher than those measured in the single-phase domains including the high-temperature region of the β-phase. The estimated stress exponent $n \approx 1.5$ given in [7] suggests that in the $(\alpha+\beta)$ domain the deformation mechanism could be controlled by "interphase interface sliding."

For the creep rate data of Zr1%Nb alloy reported in [7], due to lack of simple constitutive relations in the two-phase coexistence $(\alpha + \beta)$ domain, we have used the Ashby-Verrall model with a slight change in the creep activation energy, relative to that of Zircaloy-4, and we obtained a fair agreement with experimental data, albeit a limited number of data points (39 values). In an earlier report [44] and later in [31], we evaluated the creep rate data on Zr1wt%Nb alloy reported in [7], using the mixing rule given by equation (13) in the $(\alpha+\beta)$ domain, but the outcome, as can be seen from figure 39a, was unsatisfactory. Thus, simple constitutive relations of the form given by equations (8)-(11), with parameters based on fitting a limited set of data, and a phase mixing rule, seem to be inadequate for describing the superplastic behaviour in the two-phase coexistence $(\alpha + \beta)$ domain of zirconium-base alloys. In [31], however, using the Ashby-Verrall model in the $(\alpha + \beta)$ domain (sec. 3.1) the experimental data can be captured adequately, figure 39b.

The prevailing view among the investigators in the field [5–7, 15] is that another mechanism is functioning in the $(\alpha + \beta)$ domain of zirconium alloys than in the single phase domains; namely, superplastic creep caused by grain-boundary sliding with diffusional flow

of matter, and even more, by dislocation induced creep and grain boundary migration.
Garde et al.'s investigation on the uniaxial stress-strain behaviour of Zircaloy-4 at temperatures 973 to 1673 K indicated a superplastic peak at 1123 K. They note that at 1123 K, Zircaloy structure consists of about 10% volume fraction β-Zr distributed as a thin film at the boundaries of α grains. At 1123 to 1173 K, they found that at low strain rates ($< 10^{-4}$ s^{-1}) the predominant mechanism of superplasticity was grain boundary sliding, whereas at higher strain rates ($> 10^{-4}$ s^{-1}) dislocation creep was prevailing [15]. In particular, they found that for Zircaloy-4 with an equiaxed grain structure, the value of the exponent n very much depended on the strain rate in the $(\alpha + \beta)$-Zr. For example, at 1123 K, $n \approx 1.25$ for a low strain rate of $\dot{\varepsilon} \approx 3 \times 0^{-6}$ s^{-1}, then increasing continuously to $n \approx 5$ as the strain rate was increased to $\dot{\varepsilon} \approx 2 \times 10^{-3}$ s^{-1}. For Zircaloy-4 with a basketweave (acicular) grain structure, the variation in the exponent was from $n \approx 3.3$ to $n \approx 5$ in the same span of strain rate.
Moreover, Garde et al. [15] used a single-phase Ashby-Verrall model [29], to evaluate the data presented in figure 12. However, they erroneously interpreted their Zircaloy-4 data at 1123 K (Fig. 23 of Ref. [15]) to yield $p = -1$, which in fact give $p \approx 0.94$, i.e. close to $p = 1$. The results are reproduced here in figure 40 as the applied tensile stress versus strain rate. The outcome of our calculations using their input data with $p = -1$ (green curves), which are in fair agreement with measured data for strain rates, are somewhat different than those presented in Fig. 25 of [15]. We have used a fixed value for the Burgers vector, namely, $b = 3.3$ Å; whereas this is not specified in [15]. Also the value for A in equation (4) is not explicitly given in [15], which may differ somewhat from the value we used in our evaluation $A = 3.0 \times 10^{-10}$ m^3/s. In the same figure 40, we have also depicted curves (red lines) with the double-phase Ashby-Verrall model with the input data given in [31] comprising $p = 1$. The volume fractions of the β phase for Zircaloy at $T = 1123$ K and $T = 1173$ K are calculated to be $y = 0.125$ and $y = 0.611$, respectively.
For the sake of additional comparison, we have depicted in figure 41 the retrodictions of the utilized engineering correlations (see sec. 3.2) and the Ashby-Verrall model against the measured creep rate versus applied stress data at 1173 K for Zircaloy-4 (corresponding to $y = 0.611$) with the mean grain size of 5 μm [5]; see table 2. It is seen that the Ashby-Verrall model recounts the experimental data more faithfully than the employed engineering models.
It is worth pointing out that the high temperature creep behaviours of Zircaloy-4 and Zircaloy-2 are quite similar [5], i.e., the Zircaloy-4 creep rate correlations utilized in our study should also be applicable to Zircaloy-2. The chemical compositions of Zircaloy-4 and Zircaloy-2 are similar, except for the presence of 0.055 wt% nickel in the latter alloy [45].

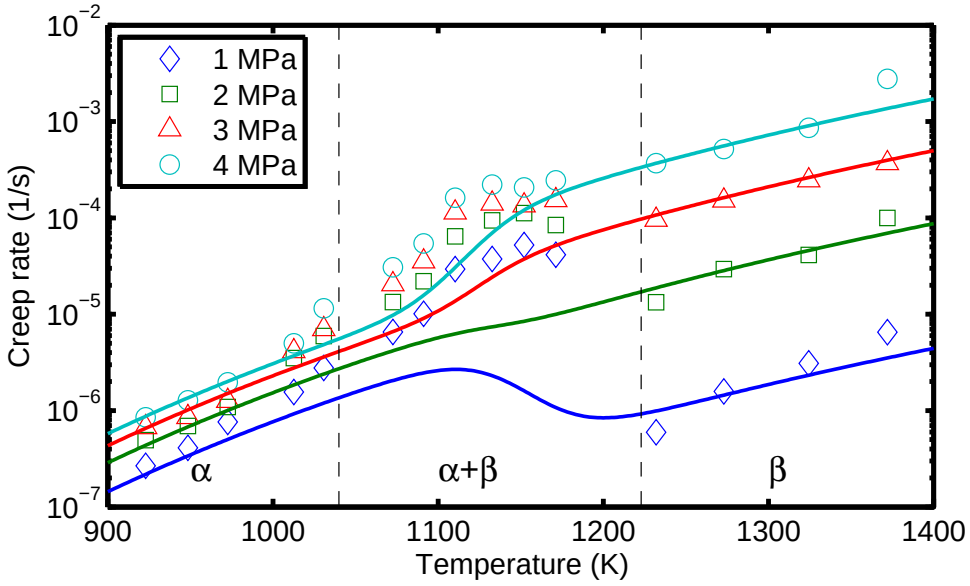

(a)

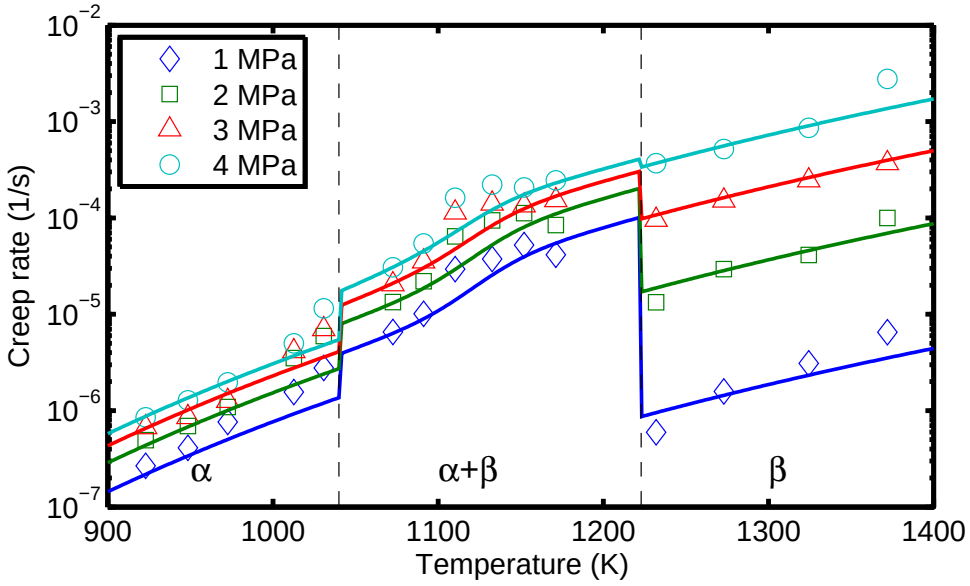

(b)

Figure 39: Creep rate of Zr1%Nb alloy versus temperature at various applied stresses [7]. The symbols are measurements while the lines are calculations according to table 8 for the α and β regions. In the $(\alpha + \beta)$ domain: (a) Eq. (13) is used to calculate the creep rate, hence indicating the inadequacy of the phase mixing rule to capture the experimental data in this domain; (b) Eqs. (6)+(7) are used; see [31].

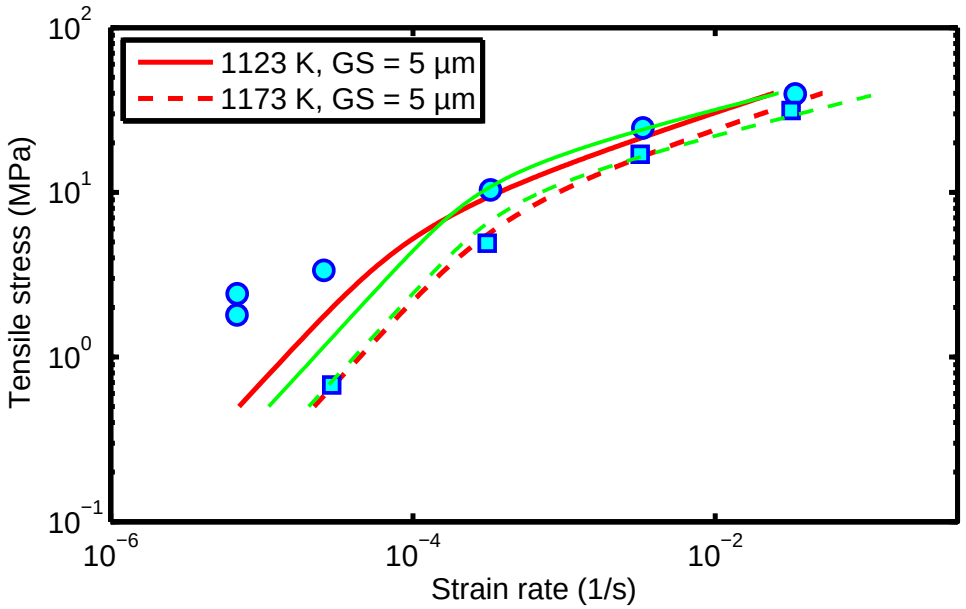

(a)

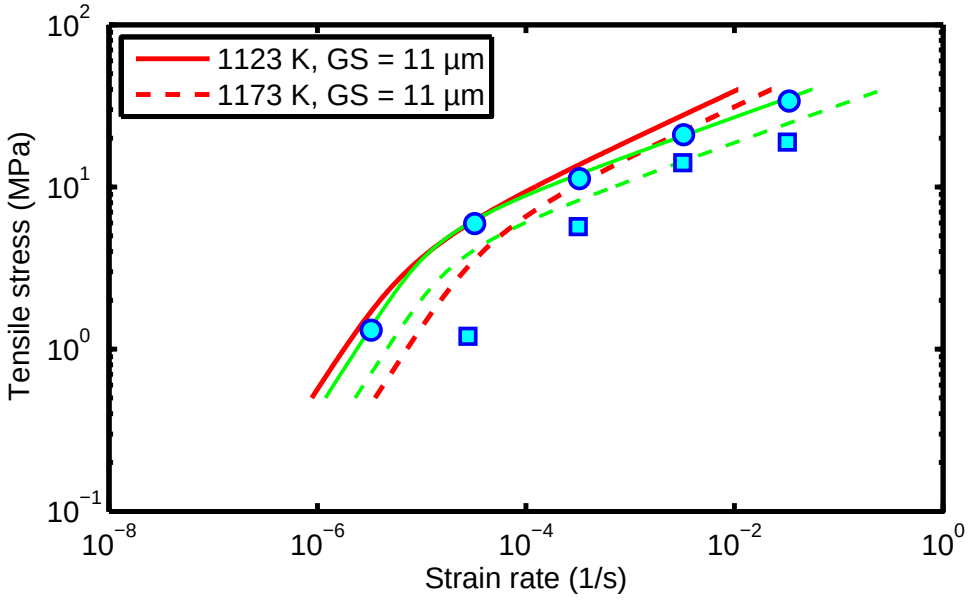

(b)

Figure 40: Comparison between the calculated (curves) and measured (markers) 0.2% yield stress versus the axial strain rate at two temperatures and two grain sizes (GS) for Zircaloy-4 (cf. figure 12); the data are adapted from [15]. The green lines are the results of single-phase Ashby-Verrall model calculations, whereas the red lines are those of two-phase Ashby-Verrall model (see the main text).

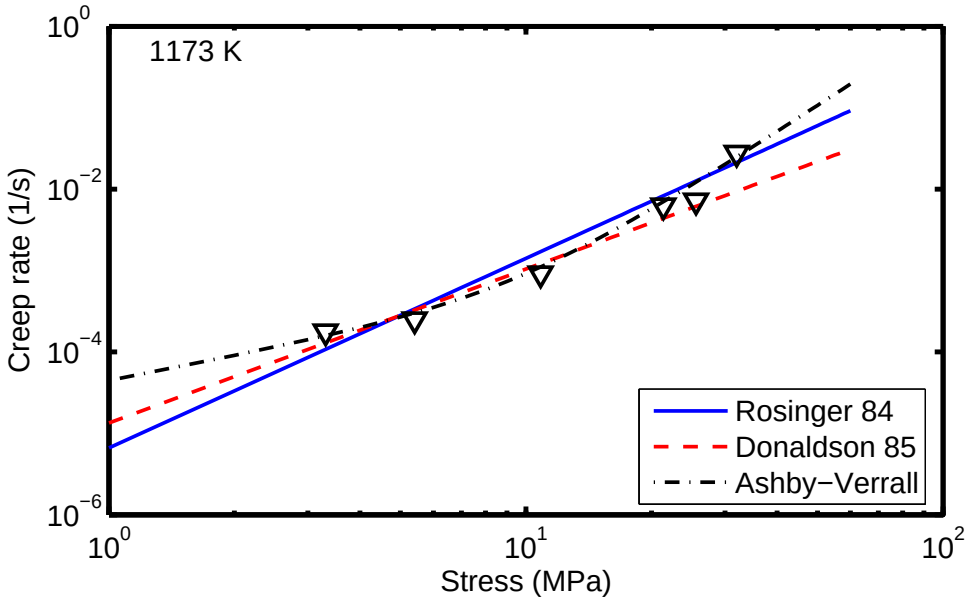

Figure 41: Comparison between the retrodictions of the used creep models (lines) and experimental data on Zircaloy-4 at 1173 K [5], cf. table 2. Axial creep strain versus nominal axial stress. Rosinger 84 is the output of Eq. (8), Donaldson 85 that of Eq. (10) and Ashby-Verrall that of Eqs. (6)+(7).

6 Conclusions

The results of our evaluation of high temperature creep data for Zircaloy-4 and Zr1%Nb alloy are summarized in table 9. The largest discrepancy between measured and calculated creep rate was found in the $(\alpha + \beta)$ domain of Zircaloy-4 using the standard creep correlations commonly used for LOCA analysis. The high temperature Zircaloy-4 cladding tube creep behaviour should also be applicable to Zircaloy-2 cladding tubes; whereas separate correlations should be used to describe creep of Zr-1wt%Nb alloy.
It is understood from the literature and the evaluations made here that for both Zircaloy-4 and Zr1%Nb alloy in the high temperature α domain, experimental data exhibit two creep regimes: At low stresses the deformation mechanism could be diffusional creep; while at higher stresses the deformation mechanism is most likely dislocation climb induced creep. In the β domain, only one regime, i.e., dislocation climb induced creep has been inferred. In the two-phase coexistence $(\alpha + \beta)$ domain, however, the creep behaviour is more complex and as such no simple creep law has been established. In the $(\alpha + \beta)$ domain the deformation mechanism could be controlled by interphase interface sliding, which is the hallmark of superplasticity. The Ashby-Verrall model for superplasticity, which is based on grain-boundary sliding with diffusional accommodation seems to be a good starting base for describing the creep behaviour in this domain. More experimental data, especially for niobium modified zirconium alloys with good material pre-characterization, would be valuable for verification and improvement of the prevailing models.

Acknowledgements

I wish to express my gratitude to Lars Olof Jernkvist for critical reading of the manuscript and comments thereof and to Tero Manngård for helpful assistance. The work was supported by the Swedish Radiation Safety Authority (SSM) under the contract number SSM 2008/139.

References

[1] P. D. Parsons, E. D. Hindle, and C. A. Mann. The deformation, oxidation and embrittlement of PWR fuel cladding in a loss-of-coolant accident. Technical Report CSNI 129, OECD Nuclear Energy Agency, Paris, France, 1986.

[2] A. R. Massih. Review of experimental data for modelling LWR fuel cladding behaviour under loss of coolant accident conditions. Technical Report 2007:14, Swedish Nuclear Power Inspectorate, Stockholm, Sweden, 2007.

[3] K. Pettersson. Nuclear fuel behaviour in loss-of-coolant (LOCA) conditions. Technical Report NEA No. 6846, OECD Nuclear Energy Agency, Issy-les-Moulineaux, France, 2009.

[4] T. Manngård and A. R. Massih. Modelling and simulation of reactor fuel cladding under loss-of-coolant conditions. *J. Nucl. Sci. Techn.*, 48:39–49, 2011.

[5] H. E. Rosinger, P. C. Bera, and W. R. Clendening. Steady-state creep of Zircaloy-4 fuel cladding from 940 to 1873 K. *J. Nucl. Mater.*, 82:286–297, 1979.

[6] A. T. Donaldson, T. Healey, and R. A. L. Horwood. Biaxial creep deformation of Zircaloy-4 PWR fuel cladding in the alpha, (alpha+beta) and beta phase temperature range. In *Proceedings of Nuclear Fuel Performance Conference*, pages 83–89, UK, 1985. British Nuclear Energy Society (BNES).

[7] D. Kaddour, S. Frechinet, A. F. Gourgues, J. C. Brachet, L. Portier, and A. Pineau. Experimental determination of creep properties of zirconium alloys together with phase transformation. *Scripta Mater.*, 51:515–519, 2004.

[8] H. E. Rosinger, P. C. Bera, and W. R. Clendening. The steady-state creep of Zircaloy-4 fuel cladding from 940 to 1873 K. Technical Report AECL-6193, Atomic Energy of Canada Limited, 1978.

[9] M.F. Osborne and G.W. Parker. The effect of irradiation on the failure of Zircaloy clad fuel rods. Technical Report ORNL-TM-3626, Oak Ridge National Laboratory, 1972.

[10] C.J. Baroch, A.V. Munim, and E.N. Harbinson. Effects of irradiation in a thermal reactor on the tensile properties of Zircaloy-2 and -4 and borated stainless steel. In *Zirconium in the Nuclear Industry*, volume ASTM STP 484, pages 176–193, Philadelphia, USA, 1970. American Society for Testing and Materials.

[11] C. Lemaignan and A. T. Motta. Zirconium alloys in nuclear applications. In R. W. Cahn, P. Haasen, and E. J. Kramer, editors, *Nuclear Materials*, volume 10B of *Materials Science and Technology*, chapter 7, pages 1–51. VCH, Weinheim, Germany, 1994. Volume editor B.R.T. Frost.

[12] A. Miquet, D. Charquet, and C. H. Allibert. Solid state phase equilibria of Zircaloy-4 in the temperature range 750-1050°C. *J. Nucl. Mater.*, 105:132–141, 1982.

[13] N. V. Bangaru, R. A. Busch, and J. H. Schemel. Effects of beta quenching on the microstructure and corrosion of Zircaloys. In R.B. Adamson and L.F.P. van Swam, editors, *Zirconium in the Nuclear Industry: Seventh International Symposium*, volume ASTM STP 939, pages 341–363, Philadelphia, USA, 1987. American Society for Testing and Materials.

[14] R. Jerlerud Peréz and A. R. Massih. Thermodynamic evaluation of the Nb-O-Zr system. *J. Nucl. Mater.*, 360:242–254, 2007.

[15] A. M. Garde, H. M. Chung, and T. F. Kassner. Micrograin superplasticity in Zircaloy at 850°C. *Acta Metall.*, 26:153–166, 1978.

[16] H. M. Chung and T. F. Kassner. Pseudobinary Zircaloy-oxygen phase diagram. *J. Nucl. Mater.*, 84:327–339, 1979.

[17] A. T. Donaldson and T. Healey. Creep deformation of Westinghouse Zircaloy-4 fuel cladding tubes in alpha plus beta phase temperature range. Technical Report TRPD/B/0564/N85, Central Electricity Generating Board, Berkeley, Gloucestershire, UK, 1984.

[18] A. T. Donaldson, T. Healey, and R. A. L. Horwood. Creep behaviour of Westinghouse Zr-4 fuel between 973 and 1073 K. Technical Report TRPD/B/0008/N82, Central Electricity Generating Board, Berkeley, Gloucestershire, UK, 1985.

[19] D. A. Woodford. Constant load creep data interpreted in terms of the stress dependence of dislocation velocity. *Trans. Metall. Soc. AIME*, 239:655–659, 1967.

[20] D. A. Woodford. Analysis of creep curves for a magnesium-zirconium alloy. *J. Institute of Metals*, 96:371–374, 1968.

[21] A. M. Garde, H. M. Chung, and T. F. Kassner. Uniaxial tensile properties of Zircaloy containing oxygen: summary report. Technical Report ANL-77-30, Argonne National Laboratory, 1977.

[22] D. Lee and W. A. Backofen. Superplasticity in some titanium and zirconium alloys. *Trans. Metall. Soc. AIME*, 239:1034–1040, 1967.

[23] K. Nuttall. Superplasticity in the Zr-2.5%Nb alloy. *Scripta Metall.*, 10:835–840, 1976.

[24] M. Bocek, P. Hofmann, and C. Petersen. Superplasticity of Zircaloy-4. In A.L. Lowe and G.W. Parry, editors, *Zirconium in the Nuclear Industry*, volume ASTM STP 633, pages 66–81, Philadelphia, USA, 1977. American Society for Testing and Materials.

[25] H. E. Rosinger and A. E. Unger. The superplastic and strain-rate dependent plastic flow of zirconium-2.5 wt% niobium in the 873 to 1373 K temperature range. Technical Report AECL-6418, Atomic Energy of Canada Limited, Pinawa, Manitoba, Canada, 1979.

[26] M. E. Kassner. *Fundamentals of Creep in Metals and Alloys*. Elsevier, Amsterdam, The Netherlands, 2009. Chapter 6.

[27] A. K. Mukherjee. Superplasticity in metals, ceramics and intermetallics. In R. W. Cahn, P. Haasen, and E. J. Kramer, editors, *Plastic Deformation and Fracture of Materials*, volume 6 of *Material Science and Technology*, chapter 9, pages 1–30. VCH, Weinheim, Germany, 1993. Volume editor H. Mughrabi.

[28] T. G. Langdon. Grain boundary sliding revisited: Developments in sliding over four decades. *J. Mater. Sci.*, 41:597–609, 2006.

[29] M. F. Ashby and R. A. Verrall. Diffusion-accommodated flow and superplasticity. *Acta Metall.*, 21:149–163, 1973.

[30] A. K. Mukherjee, J. E. Bird, and J. E. Dorn. Experimental correlations for high temperature creep. *Trans. Ams. Soc. Metals*, 62:155–179, 1969.

[31] A. R. Massih. High-temperature creep and superplasticity in zirconium alloys. *J. Nucl. Sci. Techn.*, 50:21–34, 2013.

[32] H. Naziri, R. Pearce, M. Henderson-Brown, and K.F. Hale. Microstructural-mechanism relationship in the zinc/aluminium eutectoid superplastic alloy. *Acta Metall.*, 23:489–496, 1975.

[33] T. G. Langdon. The physics of superplastic deformation. *Mater. Sci. and Eng.*, A137:1–11, 1991.

[34] A. R. Massih and L. O. Jernkvist. Transformation kinetics of alloys under non-isothermal conditions. *Modelling Simul. Mater. Sci. Eng.*, 17:055002, 2009.

[35] A. R. Massih. Transformation kinetics of zirconium alloys under non-isothermal conditions. *J. Nucl. Mater.*, 384:330–335, 2009.

[36] F. J. Erbacher, H. J. Neitzel, H. Rosinger, H. Schmidt, and K. Wiehr. Burst criterion of Zircaloy fuel claddings in a loss-of-coolant accident. In D. G. Franklin, editor, *Zirconium in the Nuclear Industry: Fifth Conference*, volume ASTM STP 754, pages 271–283, Philadelphia, USA, 1982. American Society for Testing and Materials.

[37] H. E. Rosinger. A model to predict the failure of Zircaloy-4 fuel sheathing during postulated LOCA conditions. *J. Nucl. Mater.*, 120:41–54, 1984.

[38] R. Hill. A theory of yielding and plastic flow of anisotropic materials. *Proc. Roy. Soc. A*, 193:281–297, 1948.

[39] H. J. Neitzel and H. E. Rosinger. The development of a burst criterion for Zircaloy fuel cladding under LOCA conditions. Technical Report AECL-6420, Atomic Energy of Canada Limited, 1980.

[40] H. J. Frost and M. F. Ashby. *Deformation mechanism maps*. Pergamon Press, Oxford, 1982.

[41] E. N. Pirogov, M. I. Alymov, and L. L. Artyukhina. Creep of N1 alloy within the region of polymorphic transformation. *Atomic Energy*, 65:864–866, 1989. Translated from Atomnaya Energiya, Vol. 65, pp. 293-294, October 1988.

[42] P. VanUffelen, C. Győri, A. Schubert, J. van de Laar, Z. Hózer, and G. Spykman. Extending the application range of a fuel performance code from normal operating to design basis accident conditions. *J. Nucl. Mater.*, 383:137–143, 2008.

[43] D. Kaddour. Fluage isotherme et anisotherme dans les domaines monophasés (α et β) et biphasés (α + β) d'un alliage Zr-1%NbO. Doctoral dissertation, December 2004. Ecole des Mines de Paris.

[44] A. R. Massih. A model for analysis of Zr alloy fuel cladding behaviour under LOCA conditions. Technical Report TR08-007v1, Quantum Technologies AB, Uppsala, Sweden, 2009.

[45] L. M. Petrie, P. B. Fox, and K. Lucius. Standard composition library. Technical Report NUREG/CR-0200, U.S. Nuclear Regulatory Commission, Washington D.C., U.S.A., 1998. Revision 6.

2014:20

The Swedish Radiation Safety Authority has a comprehensive responsibility to ensure that society is safe from the effects of radiation. The Authority works to achieve radiation safety in a number of areas: nuclear power, medical care as well as commercial products and services. The Authority also works to achieve protection from natural radiation and to increase the level of radiation safety internationally.

The Swedish Radiation Safety Authority works proactively and preventively to protect people and the environment from the harmful effects of radiation, now and in the future. The Authority issues regulations and supervises compliance, while also supporting research, providing training and information, and issuing advice. Often, activities involving radiation require licences issued by the Authority. The Swedish Radiation Safety Authority maintains emergency preparedness around the clock with the aim of limiting the aftermath of radiation accidents and the unintentional spreading of radioactive substances. The Authority participates in international co-operation in order to promote radiation safety and finances projects aiming to raise the level of radiation safety in certain Eastern European countries.

The Authority reports to the Ministry of the Environment and has around 300 employees with competencies in the fields of engineering, natural and behavioural sciences, law, economics and communications. We have received quality, environmental and working environment certification.

Strålsäkerhetsmyndigheten
Swedish Radiation Safety Authority

SE-171 16 Stockholm
Solna strandväg 96

Tel: +46 8 799 40 00
Fax: +46 8 799 40 10

E-mail: registrator@ssm.se
Web: stralsakerhetsmyndigheten.se